



# Fischer-Tropsch Cobalt Catalyst Improvements With the Presence of $\text{TiO}_2$ , $\text{La}_2\text{O}_3$ , and $\text{ZrO}_2$ on an Alumina Support

*Jennifer Lindsey Suder Klettlinger  
Glenn Research Center, Cleveland, Ohio*

## NASA STI Program . . . in Profile

Since its founding, NASA has been dedicated to the advancement of aeronautics and space science. The NASA Scientific and Technical Information (STI) program plays a key part in helping NASA maintain this important role.

The NASA STI Program operates under the auspices of the Agency Chief Information Officer. It collects, organizes, provides for archiving, and disseminates NASA's STI. The NASA STI program provides access to the NASA Aeronautics and Space Database and its public interface, the NASA Technical Reports Server, thus providing one of the largest collections of aeronautical and space science STI in the world. Results are published in both non-NASA channels and by NASA in the NASA STI Report Series, which includes the following report types:

- **TECHNICAL PUBLICATION.** Reports of completed research or a major significant phase of research that present the results of NASA programs and include extensive data or theoretical analysis. Includes compilations of significant scientific and technical data and information deemed to be of continuing reference value. NASA counterpart of peer-reviewed formal professional papers but has less stringent limitations on manuscript length and extent of graphic presentations.
- **TECHNICAL MEMORANDUM.** Scientific and technical findings that are preliminary or of specialized interest, e.g., quick release reports, working papers, and bibliographies that contain minimal annotation. Does not contain extensive analysis.
- **CONTRACTOR REPORT.** Scientific and technical findings by NASA-sponsored contractors and grantees.

- **CONFERENCE PUBLICATION.** Collected papers from scientific and technical conferences, symposia, seminars, or other meetings sponsored or cosponsored by NASA.
- **SPECIAL PUBLICATION.** Scientific, technical, or historical information from NASA programs, projects, and missions, often concerned with subjects having substantial public interest.
- **TECHNICAL TRANSLATION.** English-language translations of foreign scientific and technical material pertinent to NASA's mission.

Specialized services also include creating custom thesauri, building customized databases, organizing and publishing research results.

For more information about the NASA STI program, see the following:

- Access the NASA STI program home page at <http://www.sti.nasa.gov>
- E-mail your question to [help@sti.nasa.gov](mailto:help@sti.nasa.gov)
- Fax your question to the NASA STI Information Desk at 443-757-5803
- Phone the NASA STI Information Desk at 443-757-5802
- Write to:  
STI Information Desk  
NASA Center for AeroSpace Information  
7115 Standard Drive  
Hanover, MD 21076-1320



# Fischer-Tropsch Cobalt Catalyst Improvements With the Presence of $\text{TiO}_2$ , $\text{La}_2\text{O}_3$ , and $\text{ZrO}_2$ on an Alumina Support

*Jennifer Lindsey Suder Klettlinger  
Glenn Research Center, Cleveland, Ohio*

National Aeronautics and  
Space Administration

Glenn Research Center  
Cleveland, Ohio 44135

## Acknowledgments

I would like to express my gratitude to my advisor Dr. Steven S. C. Chuang for his guidance and support during my thesis research. I would also like to thank Dr. Bi-min Zhang Newby and Dr. George Chase who were my committee members. I appreciate the Center for Applied Energy Research at The University of Kentucky, namely Dr. Burt Davis and Dr. Gary Jacobs for their guidance and continued support in catalyst characterization. I would also like to express my appreciation to my colleagues at NASA Glenn Research Center: Chia (Judy) Yen, Angela Surgenor, Leah Nakley, Rachel Rich, Ana De La Ree, Lauren Best, and Al Hepp for their understanding and patience during my completion of this work. I am appreciative of the support from my supervisor, Dr. Chi-Ming Lee and the funding received from NASA Glenn Research Center for completion of my thesis and graduate coursework. I am deeply grateful to my husband for his ongoing love and encouragement, as well as my parents for their dedication, encouragement, and many years of support throughout my life. The work in this thesis would not have been possible without those mentioned in the above acknowledgment.

## Supplementary Notes

This report was submitted as a thesis in partial fulfillment of the requirements for the degree of Master of Science to the graduate faculty of the University of Akron, Akron, Ohio, May 2012.

Trade names and trademarks are used in this report for identification only. Their usage does not constitute an official endorsement, either expressed or implied, by the National Aeronautics and Space Administration.

This work was sponsored by the Fundamental Aeronautics Program at the NASA Glenn Research Center.

*Level of Review:* This material has been technically reviewed by technical management.

Available from

NASA Center for Aerospace Information  
7115 Standard Drive  
Hanover, MD 21076-1320

National Technical Information Service  
5301 Shawnee Road  
Alexandria, VA 22312

Available electronically at <http://www.sti.nasa.gov>

# Fischer-Tropsch Cobalt Catalyst Improvements With the Presence of $\text{TiO}_2$ , $\text{La}_2\text{O}_3$ , and $\text{ZrO}_2$ on an Alumina Support

Jennifer Lindsey Suder Klettlinger  
National Aeronautics and Space Administration  
Glenn Research Center  
Cleveland, Ohio 44135

## ABSTRACT

The objective of this study was to evaluate the effect of titanium oxide, lanthanum oxide, and zirconium oxide on alumina supported cobalt catalysts. The hypothesis was that the presence of lanthanum oxide, titanium oxide, and zirconium oxide would reduce the interaction between cobalt and the alumina support. This was of interest because an optimized weakened interaction could lead to the most advantageous cobalt dispersion, particle size, and reducibility. The presence of these oxides on the support were investigated using a wide range of characterization techniques such as SEM, nitrogen adsorption, x-ray diffraction (XRD), temperature programmed reduction (TPR), temperature programmed reduction after reduction (TPR-AR), and hydrogen chemisorptions/pulse reoxidation. Results indicated that both  $\text{La}_2\text{O}_3$  and  $\text{TiO}_2$  doped supports facilitated the reduction of cobalt oxide species in reference to pure alumina supported cobalt catalysts, however further investigation is needed to determine the effect of  $\text{ZrO}_2$  on the reduction profile. Results showed an increased corrected cluster size for all three doped supported catalysts in comparison to their reference catalysts. The increase in reduction and an increase in the cluster size led to the conclusion that the support-metal interaction weakened by the addition of  $\text{TiO}_2$  and  $\text{La}_2\text{O}_3$ . It is also likely that the interaction decreased upon presence of  $\text{ZrO}_2$  on the alumina, but

further research is necessary. Preliminary results have indicated that the alumina-supported catalysts with titanium oxide and lanthanum oxide present are of interest because of the weakened cobalt support interaction. These catalysts showed an increased extent of reduction, therefore more metallic cobalt is present on the support. However, whether or not there is more cobalt available to participate in the Fischer-Tropsch synthesis reaction (cobalt surface atoms) depends also on the cluster size. On one hand, increasing cluster size alone tends to decrease the active site density; on the other hand, by increasing the size of the cobalt clusters, there is less likelihood of forming oxidized cobalt complexes (cobalt aluminate) during Fischer-Tropsch synthesis. Thus, from the standpoint of stability, improving the extent of reduction while increasing the particle size slightly may be beneficial for maintaining the sites, even if there is a slight decrease in overall initial active site density.

## TABLE OF CONTENTS

LIST OF TABLES .....	viii
LIST OF FIGURES .....	ix
CHAPTER	
I. INTRODUCTION.....	1
1.1 Fischer Tropsch Synthesis.....	1
1.2 Fischer-Tropsch Cobalt Catalysts .....	1
1.3 Objectives and Hypothesis.....	2
1.4 Outline.....	3
II. BACKGROUND OF THE STUDY.....	4
2.1 Principles of Cobalt Fischer-Tropsch Catalysis .....	4
2.2 Fischer-Tropsch Cobalt Catalyst Oxide Support Interaction Effect ..	5
2.3 Cobalt Metal Loading and Size.....	6
2.4 Promoter Metals.....	7
2.5 Preparation Method.....	8
2.6 Pore Size .....	9
2.7 Mixed Oxide Supports .....	9
2.7.1 Titanium oxide (TiO <sub>2</sub> ) .....	9
2.7.2 Lanthanum Oxide (La <sub>2</sub> O <sub>3</sub> ) .....	11
2.7.3 Zirconium Oxide (ZrO <sub>2</sub> ).....	13

2.8	Brunauer Emmet Teller (BET) Surface Area Measurements .....	14
2.9	Temperature Programmed Reduction and Temperature Programmed Reduction After Reduction .....	17
2.10	Hydrogen Chemisorption and Pulse Reoxidation .....	18
2.11	X-ray Diffraction.....	23
III. EXPERIMENTAL PROCEDURES.....		24
3.1	Catalyst Preparation.....	24
3.2	Catalyst Characterization.....	29
3.2.1	Scanning Electron Microscopy and Electron Dispersed Spectroscopy .....	29
3.2.2	Brunauer Emmet Teller (BET) Surface Area Measurements and Barrett Joyner Halenda (BJH) Pore Size Distributions.....	30
3.2.3	Temperature Programmed Reduction (TPR).....	30
3.2.4	Temperature Programmed Reduction After Reduction .....	31
3.2.5	Hydrogen Chemisorption with Pulse Reoxidation .....	31
3.2.6	X-ray Diffraction.....	32
IV. CATALYST CHARACTERIZATION RESULTS .....		34
4.1	Scanning Electron Microscopy and Electron Dispersed Spectroscopy .....	34
4.2	Brunauer Emmet Teller (BET) <sup>4</sup> and Barrett Joyner Halenda (BJH) <sup>33</sup> Measurements.....	45
4.3	Temperature Programmed Reduction .....	50

4.4	Temperature Programmed Reduction After Reduction (TPR-AR)	55
4.5	Hydrogen Chemisorption .....	57
4.6	X-Ray Diffraction (XRD) .....	65
4.7	Discussion.....	70
4.8	Conclusions .....	74
	BIBLIOGRAPHY.....	77
	APPENDIX A. Pore Size Distribution Profiles.....	80

## LIST OF TABLES

Table	Page
2.1 BET Data from Literature .....	16
2.2 Hydrogen Chemisorption Data from Literature .....	20
2.3 XRD Data from Literature.....	23
3.1 Catalyst support composition.....	25
4.1 Scanning Electron Microscopy-Energy Dispersive Spectroscopy (SEM-EDS) quantitative results for 9.7%TiO <sub>2</sub> -Al <sub>2</sub> O <sub>3</sub> .....	38
4.2 Scanning Electron Microscopy-Energy Dispersive Spectroscopy (SEM-EDS) quantitative results for 3.0%La <sub>2</sub> O <sub>3</sub> -Al <sub>2</sub> O <sub>3</sub> .....	41
4.3 Scanning Electron Microscopy-Energy Dispersive Spectroscopy (SEM-EDS) quantitative results for 3.1%ZrO <sub>2</sub> -Al <sub>2</sub> O <sub>3</sub> .....	44
4.4 BET surface area measurements and BJH pore volume and pore radius measurements.....	49
4.5 Hydrogen chemisorption / pulse reoxidation results following 10 hour hydrogen reduction at 350°C.....	64
4.6 X-ray Diffraction results from XRD plots and Scherrer Equation.....	70

## LIST OF FIGURES

Figure	Page
3.1 Calcination reactor drawing.....	27
4.1 Scanning Electron Microscopy-Energy Dispersive Spectroscopy (SEM-EDS) mapping results for 9.7%TiO <sub>2</sub> -Al <sub>2</sub> O <sub>3</sub> where Al <sub>2</sub> O <sub>3</sub> is pink (left) and TiO <sub>2</sub> is green (right).....	35
4.2 Scanning Electron Microscopy-Energy Dispersive Spectroscopy (SEM-EDS) mapping results overlaid on scanning electron microscopy image for 9.7%TiO <sub>2</sub> -Al <sub>2</sub> O <sub>3</sub> where Al <sub>2</sub> O <sub>3</sub> is pink (left) and TiO <sub>2</sub> is green (right). .....	36
4.3 Scanning Electron Microscopy-Energy Dispersive Spectroscopy (SEM-EDS) mapping results for 9.7%TiO <sub>2</sub> -Al <sub>2</sub> O <sub>3</sub> overlaid on scanning electron microscopy image. Alumina is highlighted in pink and titania is highlighted in green.....	37
4.4 Scanning Electron Microscopy-Energy Dispersive Spectroscopy (SEM-EDS) quantitative results for 9.7%TiO <sub>2</sub> -Al <sub>2</sub> O <sub>3</sub> support.....	38
4.5 Scanning Electron Microscopy-Energy Dispersive Spectroscopy (SEM-EDS) mapping results for 3.0%La <sub>2</sub> O <sub>3</sub> -Al <sub>2</sub> O <sub>3</sub> where Al <sub>2</sub> O <sub>3</sub> is pink (left) and La <sub>2</sub> O <sub>3</sub> is green (right).....	39
4.6 Scanning Electron Microscopy-Energy Dispersive Spectroscopy (SEM-EDS) mapping results overlaid on scanning electron microscopy image for 3.0%La <sub>2</sub> O <sub>3</sub> -Al <sub>2</sub> O <sub>3</sub> where Al <sub>2</sub> O <sub>3</sub> is pink (left) and La <sub>2</sub> O <sub>3</sub> is green (right).....	40
4.7 Scanning Electron Microscopy-Energy Dispersive Spectroscopy (SEM-EDS) mapping results for 3.0%La <sub>2</sub> O <sub>3</sub> -Al <sub>2</sub> O <sub>3</sub> overlaid on scanning electron microscopy image (Al <sub>2</sub> O <sub>3</sub> in pink and La <sub>2</sub> O <sub>3</sub> in green).....	40
4.8 Scanning Electron Microscopy-Energy Dispersive Spectroscopy (SEM-EDS) Quantitative Results for 3.0%La <sub>2</sub> O <sub>3</sub> -Al <sub>2</sub> O <sub>3</sub> .....	41
4.9 Scanning Electron Microscopy-Energy Dispersive Spectroscopy (SEM-EDS) mapping results for 3.1%ZrO <sub>2</sub> -Al <sub>2</sub> O <sub>3</sub> where Al <sub>2</sub> O <sub>3</sub> is pink (left) and ZrO <sub>2</sub> is green (right).....	42

4.10	Scanning Electron Microscopy-Energy Dispersive Spectroscopy (SEM-EDS) mapping results overlaid on scanning electron microscopy image for 3.1%ZrO <sub>2</sub> -Al <sub>2</sub> O <sub>3</sub> where Al <sub>2</sub> O <sub>3</sub> is pink (left) and ZrO <sub>2</sub> is green (right).....	42
4.11	Scanning Electron Microscopy-Energy Dispersive Spectroscopy (SEM-EDS) mapping results for 3.1%ZrO <sub>2</sub> -Al <sub>2</sub> O <sub>3</sub> overlaid on scanning electron microscopy image where Al <sub>2</sub> O <sub>3</sub> is pink (left) and ZrO <sub>2</sub> is green (right).....	43
4.12	Scanning Electron Microscopy-Energy Dispersive Spectroscopy (SEM-EDS) Quantitative Results for 3.1%ZrO <sub>2</sub> -Al <sub>2</sub> O <sub>3</sub> .....	44
4.13	Expected BET surface areas of (a) 15%Co/9.7%TiO <sub>2</sub> -Al <sub>2</sub> O <sub>3</sub> , (b) 15%Co/3.0%La <sub>2</sub> O <sub>3</sub> -Al <sub>2</sub> O <sub>3</sub> , (c) 15%Co/3.1%ZrO <sub>2</sub> -Al <sub>2</sub> O <sub>3</sub> .....	46
4.14	BET surface area comparison of (a) 15%Co/9.7%TiO <sub>2</sub> -Al <sub>2</sub> O <sub>3</sub> , (b) 15%Co/3.0%La <sub>2</sub> O <sub>3</sub> -Al <sub>2</sub> O <sub>3</sub> , (c) 15%Co/3.1%ZrO <sub>2</sub> -Al <sub>2</sub> O <sub>3</sub> , (d) 15%Co/Al <sub>2</sub> O <sub>3</sub> HP14/150, (e) 15%Co/Al <sub>2</sub> O <sub>3</sub> SBA150, and (f) 15%Co/Al <sub>2</sub> O <sub>3</sub> SBA200.....	47
4.15	Barrett Joyner Halenda (BJH) average pore radius adsorption data for (a) 15%Co/9.7%TiO <sub>2</sub> -Al <sub>2</sub> O <sub>3</sub> , (b) 15%Co/3.0%La <sub>2</sub> O <sub>3</sub> -Al <sub>2</sub> O <sub>3</sub> , (c) 15%Co/3.1%ZrO <sub>2</sub> -Al <sub>2</sub> O <sub>3</sub> , (d) 15%Co/Al <sub>2</sub> O <sub>3</sub> HP14/150, (e) 15%Co/Al <sub>2</sub> O <sub>3</sub> SBA150, and (f) 15%Co/Al <sub>2</sub> O <sub>3</sub> SBA200. ....	48
4.16	Barrett Joyner Halenda (BJH) average pore volume desorption data for (a) 15%Co/9.7%TiO <sub>2</sub> -Al <sub>2</sub> O <sub>3</sub> , (b) 15%Co/3.0%La <sub>2</sub> O <sub>3</sub> -Al <sub>2</sub> O <sub>3</sub> , (c) 15%Co/3.1%ZrO <sub>2</sub> -Al <sub>2</sub> O <sub>3</sub> , (d) 15%Co/Al <sub>2</sub> O <sub>3</sub> HP14/150, (e) 15%Co/Al <sub>2</sub> O <sub>3</sub> SBA150, and (f) 15%Co/Al <sub>2</sub> O <sub>3</sub> SBA200. ....	48
4.17	H-TPR profiles of, moving upward, (a) 15%Co/9.7%TiO <sub>2</sub> -Al <sub>2</sub> O <sub>3</sub> ; (b) 15%Co/3.0%La <sub>2</sub> O <sub>3</sub> -Al <sub>2</sub> O <sub>3</sub> ; and (c) 15%Co/3.1%ZrO <sub>2</sub> -Al <sub>2</sub> O <sub>3</sub> .....	51
4.18	H-TPR profiles of, moving upward, (a) 15%Co/9.7%TiO <sub>2</sub> -Al <sub>2</sub> O <sub>3</sub> , (b) 15%Co/Al <sub>2</sub> O <sub>3</sub> SBA 150, and (c) 15%Co/Al <sub>2</sub> O <sub>3</sub> HF14/150 .....	52
4.19	H-TPR profiles of, moving upward, (a) 15%Co/Al <sub>2</sub> O <sub>3</sub> SBA 150, (b) 15%Co/3.0%La <sub>2</sub> O <sub>3</sub> -Al <sub>2</sub> O <sub>3</sub> , and (c) 15%Co/Al <sub>2</sub> O <sub>3</sub> SBA 200.....	53
4.20	H-TPR profiles of, moving upward, (a) 15%Co/Al <sub>2</sub> O <sub>3</sub> SBA 150; (b) 15%Co/3.1%ZrO <sub>2</sub> -Al <sub>2</sub> O <sub>3</sub> and (c) 15%Co/Al <sub>2</sub> O <sub>3</sub> SBA 200. ....	54
4.21	H-TPR profiles of, moving upward, (a) 15%Co/9.7%TiO <sub>2</sub> -Al <sub>2</sub> O <sub>3</sub> , (b) 15%Co/3.0%La <sub>2</sub> O <sub>3</sub> -Al <sub>2</sub> O <sub>3</sub> , (c) 15%Co/3.1%ZrO <sub>2</sub> -Al <sub>2</sub> O <sub>3</sub> , (d) 15%Co/Al <sub>2</sub> O <sub>3</sub> HP14/150, (e) 15%Co/Al <sub>2</sub> O <sub>3</sub> SBA150, and (f) 15%Co/Al <sub>2</sub> O <sub>3</sub> SBA200.....	54

4.22	H-TPR (solid) and (dashed) H-TPR-AR profiles of, moving upward, (a) 15%Co/9.7%TiO <sub>2</sub> -Al <sub>2</sub> O <sub>3</sub> ; (b) 15%Co/3.0%La <sub>2</sub> O <sub>3</sub> -Al <sub>2</sub> O <sub>3</sub> ; and (c) 15%Co/3.1%ZrO <sub>2</sub> -Al <sub>2</sub> O <sub>3</sub> . Reduction was carried out in hydrogen for 10 hours at 350°C. ....	55
4.23	H-TPR (solid) and (dashed) H-TPR-AR profiles of, moving upward, (a) 15%Co/9.7%TiO <sub>2</sub> -Al <sub>2</sub> O <sub>3</sub> , (b) 15%Co/3.0%La <sub>2</sub> O <sub>3</sub> -Al <sub>2</sub> O <sub>3</sub> , (c) 15%Co/3.1%ZrO <sub>2</sub> -Al <sub>2</sub> O <sub>3</sub> , (d) 15%Co/Al <sub>2</sub> O <sub>3</sub> HP14/150, (e) 15%Co/Al <sub>2</sub> O <sub>3</sub> SBA150, and (f) 15%Co/Al <sub>2</sub> O <sub>3</sub> SBA200. ....	56
4.24	Temperature programmed desorption data for comparison of all catalysts with their corresponding reference catalysts. ....	59
4.25	Extent of reduction results from pulse reoxidation testing for each catalyst in comparison to its corresponding reference catalyst. ....	60
4.26	Pulse reoxidation cluster size data, which is corrected for extent of reduction for each catalyst in comparison to its reference catalysts. ....	61
4.27	Corrected dispersion data for each catalyst in comparison to its reference catalysts. ....	62
4.28	X-ray diffraction profile of 15%Co/9.7%TiO <sub>2</sub> -Al <sub>2</sub> O <sub>3</sub> (a) and 9.7%TiO <sub>2</sub> -Al <sub>2</sub> O <sub>3</sub> (b). ....	65
4.29	X-ray diffraction profiles of 15%Co/3.0%La <sub>2</sub> O <sub>3</sub> -Al <sub>2</sub> O <sub>3</sub> (a) and 3.0%La <sub>2</sub> O <sub>3</sub> -Al <sub>2</sub> O <sub>3</sub> (b). ....	66
4.30	X-ray diffraction patterns of calcined samples 15%Co/3.1%ZrO <sub>2</sub> -Al <sub>2</sub> O <sub>3</sub> (a) and 3.1%ZrO <sub>2</sub> -Al <sub>2</sub> O <sub>3</sub> (b). ....	67
4.31	X-ray diffraction patterns of calcined samples 15%Co/Al <sub>2</sub> O <sub>3</sub> HP14/150 (a) and Al <sub>2</sub> O <sub>3</sub> HP14/150 (b). ....	68
4.32	X-ray diffraction patterns of calcined samples 15%Co/Al <sub>2</sub> O <sub>3</sub> SBA150 (a) and Al <sub>2</sub> O <sub>3</sub> SBA150 (b). ....	68
4.33	X-ray diffraction patterns of calcined samples 15%Co/Al <sub>2</sub> O <sub>3</sub> SBA200 (a) and Al <sub>2</sub> O <sub>3</sub> SBA200 (b). ....	69
4.34	Adsorption pore size distribution of (left) 9.7%TiO <sub>2</sub> -Al <sub>2</sub> O <sub>3</sub> and (right) 15%Co/9.7%TiO <sub>2</sub> -Al <sub>2</sub> O <sub>3</sub> . ....	80
4.35	Desorption pore size distributions of 9.7%TiO <sub>2</sub> -Al <sub>2</sub> O <sub>3</sub> (left) and 15%Co/9.7%TiO <sub>2</sub> -Al <sub>2</sub> O <sub>3</sub> (right).....	80

4.36	Adsorption pore size distribution of 3.0%La <sub>2</sub> O <sub>3</sub> -Al <sub>2</sub> O <sub>3</sub> (left) and 15%Co/3.0%La <sub>2</sub> O <sub>3</sub> -Al <sub>2</sub> O <sub>3</sub> (right) .....	80
4.37	Desorption pore size distribution of 3.0%La <sub>2</sub> O <sub>3</sub> -Al <sub>2</sub> O <sub>3</sub> (left) and 15%Co/3.0%La <sub>2</sub> O <sub>3</sub> -Al <sub>2</sub> O <sub>3</sub> (right).....	81
4.38	Adsorption pore size distribution of 3.1%ZrO <sub>2</sub> -Al <sub>2</sub> O <sub>3</sub> (left) and 15%Co/3.1%ZrO <sub>2</sub> -Al <sub>2</sub> O <sub>3</sub> (right) .....	81
4.39	Desorption pore size distributions of 3.1%ZrO <sub>2</sub> -Al <sub>2</sub> O <sub>3</sub> (left) and 15%Co/3.1%ZrO <sub>2</sub> -Al <sub>2</sub> O <sub>3</sub> (right). .....	81
4.40	Adsorption pore size distribution of Al <sub>2</sub> O <sub>3</sub> HP14/150 (a)& (b) and 15%Co/Al <sub>2</sub> O <sub>3</sub> HP14/150 (c) & (d). .....	82
4.41	Desorption pore size distribution of Al <sub>2</sub> O <sub>3</sub> HP14/150 (a)& (b) and 15%Co/Al <sub>2</sub> O <sub>3</sub> HP14/150 (c) & (d). .....	83
4.42	Adsorption pore size distributions of (a) & (b): SBA 150 Al <sub>2</sub> O <sub>3</sub> and (c) & (d): 15%Co/SBA 150 Al <sub>2</sub> O <sub>3</sub> . .....	84
4.43	Desorption pore size distributions of (a) & (b): SBA 150 Al <sub>2</sub> O <sub>3</sub> and (c) & (d): 15%Co/SBA 150 Al <sub>2</sub> O <sub>3</sub> . .....	85
4.44	Adsorption pore size distributions of (a) & (b): Al <sub>2</sub> O <sub>3</sub> .SBA 200 and (c) & (d): 15%Co/Al <sub>2</sub> O <sub>3</sub> .SBA 200 .....	86
4.45	Desorption pore size distributions of (a) & (b): Al <sub>2</sub> O <sub>3</sub> .SBA 200 and (c) & (d): 15%Co/Al <sub>2</sub> O <sub>3</sub> .SBA 200 .....	87

# CHAPTER I

## INTRODUCTION

### 1.1 Fischer Tropsch Synthesis

The Fischer-Tropsch process has three distinct steps: gasification, synthesis, and product upgrade. The gasification step produces syngas (hydrogen and carbon monoxide) from many carbon resources. The synthesis involves the conversion of syngas to syn-crude. Product upgrade processes the syn-crude and separates it into useable liquid fuels. The synthesis step can be optimized to increase yields and reduce energy inputs into the overall process.

### 1.2 Fischer-Tropsch Cobalt Catalysts

Cobalt-based Fischer-Tropsch catalysts are typically cobalt oxides on various ceramic supports (e.g., alumina, silica, titanium oxide, etc). The support adds mechanical stability, as well as an increased surface area for dispersion of the active metal, cobalt. Support modification can change the interaction of the cobalt with the support in order to increase activity and selectivity to the desired product. The supported cobalt catalyst requires a reduction treatment to convert cobalt oxides to metallic cobalt which catalyzes F-T synthesis reactions. This reduction step

becomes a very important step in the process and the development of the cobalt based catalysts and potentially their modified supports.

### 1.3 Objectives and Hypothesis

The objective of the presented work is to evaluate the effect of a few structural promoters in the form of oxides on alumina supported cobalt catalysts. Of these structural promoters, the modification of alumina with titanium, lanthanum, and zirconium were the focus. The presence of these oxides on the support was investigated using a wide range of characterization techniques such as SEM, nitrogen adsorption, x-ray diffraction (XRD), temperature programmed reduction (TPR), temperature programmed reduction after reduction (TPR-AR), and hydrogen chemisorptions/pulse reoxidation. These characterization techniques were used as a screening mechanism for the variety of cobalt/mixed oxide catalysts. Since the physical properties of these mixed oxide supports were inherently different, three different baseline alumina supported catalysts were used as reference catalysts. The presence of these structural promoters in the form of oxides could modify the alumina support properties and weaken the interaction of cobalt with alumina. An optimized weakened interaction could lead to the most advantageous cobalt dispersion, particle size, and reducibility. This optimization could maintain the high number of active sites, while minimizing cobalt aluminate formation. The hypothesis is that the presence of titanium oxide, lanthanum oxide,

and zirconium oxide will reduce the interaction between cobalt and the alumina support.

#### 1.4 Outline

Chapter II will provide an extensive literature survey and provide background information on the topic of interest. Previous research is presented in the area of titanium, lanthanum, and zirconium as both a structural and reduction promoter on alumina and similar ceramic supports. Chapter III provides the experimental procedures used in making the catalysts and the characterization of the catalysts in this research. Chapter IV provides all characterization results on the three improved catalysts, as well as the three reference catalysts, as well as discussion and conclusions.

## CHAPTER II

### BACKGROUND OF THE STUDY

#### 2.1 Principles of Cobalt Fischer-Tropsch Catalysis

Fischer-Tropsch (F-T) synthesis takes gaseous hydrogen and carbon monoxide and converts it into various hydrocarbon chain length product distributions. It is considered a network of parallel and consecutive reactions which take place on the surface and in the pores of catalysts<sup>5</sup>. Cobalt based catalysts have good activity and selectivity<sup>6</sup> and are known to produce high molecular weight paraffinic waxes that can be hydrocracked to produce lubricants and diesel fuels, which make them of high interest in F-T synthesis. The use of supported cobalt catalysts in F-T synthesis has led to complex development of catalyst design. Changes in support, support modifications/promotion, cobalt loading and additional promoter metals have been shown to change the performance of these catalysts drastically.

## 2.2 Fischer-Tropsch Cobalt Catalyst Oxide Support Interaction Effect

In order to increase the cobalt active sites, the cobalt metal is dispersed as clusters on high surface area supports, typically oxides or mixed oxides. The oxides are of particular interest because they are a highly porous structure, which is theoretically inert in the F-T reaction. The physical properties of the supports help increase surface area and distribute the cobalt metal clusters over the surface of the support. The dispersion of active metal on the catalyst support is dependent on the interaction of the support with the active metal, in this case cobalt. If the support has a strong interaction with cobalt, it is likely that the cobalt will be highly dispersed in small clusters on the surface of the oxide support. The support type and physical properties determine the number of active sites after reduction, and also influence the percentage of cobalt oxide species that can be reduced<sup>7</sup>.

Many different oxides can be used as the support for cobalt catalysts in Fischer-Tropsch synthesis. A few of the most common supports are  $\text{SiO}_2$ ,  $\text{TiO}_2$ , and  $\text{Al}_2\text{O}_3$ ; each of which has its own advantages and disadvantages.  $\text{Al}_2\text{O}_3$  has a strong interaction with cobalt,  $\text{TiO}_2$  has a moderate interaction with cobalt, and  $\text{SiO}_2$  has a weak interaction with cobalt<sup>8</sup>. Khodakov et al. show that the second reduction step ( $\text{CoO}$  to  $\text{Co}^0$ ) is strongly influenced by the cobalt particle size, such that smaller and more interacting particles (6nm) are more difficult to reduce than larger cluster sizes (20-70nm) in studying  $\text{SiO}_2$  as the support<sup>9</sup>. These interactions play an important role in the activity of the catalysts because of the tendency to form cobalt-oxide complexes such as cobalt aluminate, cobalt silicate, or cobalt titanate. For example,  $\text{TiO}_2$  has a strong metal-support interaction with cobalt, which makes  $\text{TiO}_2$

catalysts difficult to reduce<sup>3</sup>. This has been attributed to the strong cobalt-oxide interaction with the support and shifts the reduction temperature to much higher than preferred<sup>3</sup>. The properties of the support have been shown to play a role in the F-T kinetics<sup>8</sup> and have been linked to the catalytic performance. It is in the best interest of researchers to determine a means to reduce the use of promoters and expensive metals, while at the same time increasing the performance of these cobalt catalysts<sup>3</sup>.

Alumina tends to be favorable due to the mechanical properties<sup>10</sup>, particularly in applications such as continuously stirred tank reactors<sup>11</sup> where agitation is present. Previous research has shown that alumina supported cobalt does not completely reduce from cobalt oxide to cobalt metal because of the high cobalt metal-support interactions<sup>7</sup>. This high interaction of alumina with cobalt<sup>11</sup> results in the tendency to form cobalt aluminate species, which is likely inactive cobalt. With cobalt aluminate formation, usually cobalt loadings need to be higher than 20% in order to achieve desired activity.

### 2.3 Cobalt Metal Loading and Size

Increasing the cobalt loading on alumina has been shown to decrease the reduction temperature in both unpromoted and promoted catalysts. The cobalt cluster size has been linked to the interaction of cobalt with the support<sup>8</sup>, where having a very strong interaction of cobalt with the support results in small cluster sizes and a very dispersed active metal on the surface of the catalyst.

Wang and Chen <sup>12</sup> showed that when low loadings of cobalt are used, cobalt aluminate is favored. Cobalt aluminate can only be reduced at high reduction temperatures, which aren't feasible because of cobalt agglomeration. Their research also indicated that higher loadings of cobalt resulted with  $\text{Co}_3\text{O}_4$  crystallites that were easier to reduce, showing a single broadened TPR peak<sup>12</sup>. It has also been shown that the cluster size and the support effect play a role in the F-T kinetics<sup>8</sup> and that the kinetic reaction orders vary based on the size of the metal crystallites<sup>13</sup>.

#### 2.4 Promoter Metals

One key concern with handling cobalt based catalysts is that the active form of catalyst is in a reduced state, metallic cobalt, which oxidizes readily in air. Therefore, cobalt catalysts require a reduction step before F-T synthesis can occur. Since some cobalt-support interactions are high, it becomes difficult to fully reduce the available cobalt metal on the surface of the support. Noble metals, such as Ru, Pt, and Re are commonly added as reduction promoters in order to produce more cobalt metal surface sites by facilitating reduction of cobalt species that interact with the support<sup>14</sup>. In most cases, the application of a promoter is used in order to enhance the reduction of cobalt oxide ( $\text{CoO}$ ) to cobalt metal ( $\text{Co}^0$ ). The addition of the platinum to the surface of a  $\text{Co}/\text{Al}_2\text{O}_3$  catalyst has been proven to decrease the reduction temperature of the catalysts, most likely due to hydrogen spillover from the metallic promoter<sup>7</sup>. It has been found that the addition of Pt promoter to the

cobalt catalyst not only enhances the reducibility of the clusters, it also causes a small decrease in cobalt cluster size<sup>7</sup>.

## 2.5 Preparation Method

In cobalt catalyst synthesis, there are many different ways to load the cobalt onto the ceramic support. Some of the common methods are: impregnation, coprecipitation, sol-gel, chemical vapor deposition, and plasma<sup>15</sup>. Of these ways, impregnation is one of the most popular, having two common impregnation methods: incipient wetness impregnation (IWI) and slurry phase impregnation. Previous research has shown that incipient wetness impregnation procedures have been found to produce a wider range of cluster sizes than the slurry phase impregnation procedure<sup>7</sup>. It is widely accepted that TiO<sub>2</sub> as a support leads to a stronger cobalt- support interaction than SiO<sub>2</sub><sup>16</sup>, but it was found that the addition of TiO<sub>2</sub> to SiO<sub>2</sub> only improved catalyst performance when applying 3 out of 4 preparation techniques<sup>16</sup>. Improvements were found in precipitation, impregnation, and hydrolysis-reflux, although not in sol-gel methods<sup>16</sup>. It has been shown in other instances that preparation procedure can change the outcome of the results, which should be considered in the evaluation of the structural promoter discussion in this work.

## 2.6 Pore Size

The pore size of the ceramic support is important because it allows for the diffusion of reagents and products inside the catalyst channels and pores. This means that the pore size could limit the reaction, or possibly favor one reaction over another in F-T synthesis. Khodakov et. al <sup>15</sup> express that support pore size could affect the diffusion and capillary condensation of products in these pores and that narrow pores are more likely to be filled with liquid products than the wider pores in the catalyst. Liu et al found that the pore size of SiO<sub>2</sub> supports greatly influence the activity of the catalyst in a 0.5L CSTR<sup>17</sup>. Their research showed an optimum average pore size of 10nm in order to increase the activity<sup>17</sup>.

## 2.7 Mixed Oxide Supports

Much research has been done in the area of mixed oxide supports. The focus has been on SiO<sub>2</sub> and TiO<sub>2</sub> supports, however some research has been done on Al<sub>2</sub>O<sub>3</sub>.

### 2.7.1 Titanium oxide (TiO<sub>2</sub>)

Titanium oxide has been used as a ceramic support alone in F-T catalysis. It has a high interaction with cobalt, although not as high as alumina. In one study, the addition of TiO<sub>2</sub> to SiO<sub>2</sub> catalyst supports had drastically affected the structure and catalytic performance of the cobalt F-T catalysts<sup>16</sup>, likely by modification of the interaction between cobalt and silica. Preliminary results indicate that

impregnation method resulted in the highest activity and selectivity for C5+<sup>16</sup>. The preparation procedures had drastic affected the reduction profiles of these catalyst, through addition of a third (small) peak, which the authors attributed to an interaction compound<sup>16</sup>. This indicates that TiO<sub>2</sub> promoted catalysts were more difficult to reduce<sup>16</sup>, which is expected since TiO<sub>2</sub> has a stronger interaction with cobalt. The cobalt particle size decreased upon addition of TiO<sub>2</sub><sup>16</sup>, which was expected since smaller particles are also considered to interact more strongly with the support and be more difficult to reduce. The XRD profile showed slightly broader peaks for Co<sub>3</sub>O<sub>4</sub> crystallites on the TiO<sub>2</sub> promoted catalysts<sup>16</sup> and using the Scherrer equation, the silica only supported catalyst was found to have the largest Co<sub>3</sub>O<sub>4</sub> crystallite sizes<sup>16</sup>. These results confirm that the stronger interaction between titania and cobalt produce higher dispersed catalysts with smaller cobalt particles and that the addition of TiO<sub>2</sub> to silica support can provide an added benefit to the catalyst surface composition.

Wan et al. found a clear change in morphology from pure Al<sub>2</sub>O<sub>3</sub> by the addition of TiO<sub>2</sub> to the surface by the sol-gel method, where with increasing TiO<sub>2</sub> weight percent, XRD profiles indicate an increase in peak intensity in anatase<sup>18</sup>, which signifies an increase in TiO<sub>2</sub> cluster size. It is important that the oxide dopant is well dispersed for a uniform structure and more predictable catalytic activity.

### 2.7.2 Lanthanum Oxide (La<sub>2</sub>O<sub>3</sub>)

Lanthanum has also been known to increase activity in Fischer-Tropsch synthesis. A study by Vada et al. concludes that La<sup>3+</sup> increased the overall activity and chain-growth probability when a low loading of La<sup>3+</sup> (La/Co=0.05) was present on a Co/Al<sub>2</sub>O<sub>3</sub> catalyst, however methane production increased as well<sup>19</sup>. The authors of this study also found that the catalyst activity decreased with higher loadings of La (La/Co≥0.10)<sup>19</sup>. Since methane is not a desirable product in F-T synthesis, these results indicate that there is likely a positive and negative effect of lanthanum as a structural promoter on F-T cobalt alumina supports, which may be dependent on the amount of cobalt loaded on the support. There is significant need to determine the optimal loading of lanthanum on alumina, as well as the preparation procedure. Further investigation is necessary in order to determine the physical and kinetic influence of lanthanum as an oxide support modification.

The preparation procedure for loading lanthanum on alumina was studied by Ledford et al. and found that there was only a significant change in reducibility and cobalt metal dispersion when La<sup>3+</sup> was impregnated before cobalt loading<sup>20</sup>. The authors also determined that higher La<sup>3+</sup> loadings (La/Al>0.026) resulted in formation of a La-Co mixed oxide and enhanced the dispersion of cobalt on the La-Al<sub>2</sub>O<sub>3</sub><sup>20</sup>. The increase in dispersion showed little correlation to the reducibility in this study and the effect of increased dispersion on reducibility should be further explored.

Cai et al. also compared preparation procedures by preparing La<sub>2</sub>O<sub>3</sub>-doped alumina catalysts through impregnation and co-precipitation and found that the co-precipitation method reduced more readily and resulted in higher F-T synthesis activity and lower methane selectivity<sup>21</sup>. DRIFTS studies indicated that CO adsorbed most easily on the co-precipitated support catalyst than on the SASOL commercial support<sup>21</sup>.

Zhang et al. promoted titania with lanthanum nitrate at varying atomic ratios of La/Ti, calcined the support to drive off the nitrate and proceeded to load 12% cobalt to the La promoted Ti<sup>22</sup>. They found that as the La content increased, the cluster size of Co<sub>3</sub>O<sub>4</sub> decreased, while the percent reduction increased<sup>22</sup>. This was not to be expected because typically, larger clusters reduce easier. It appears that as the La loading increases, the reduction peak narrows and shifts to a lower temperature. It is also interesting to note that the nitrate peak shifted to a higher temperature and the area increased as the La loading increased, which was explained as a possible stabilization of nitrate during the calcination process<sup>22</sup>. The authors found that La inhibits nitrate degradation during calcination and may require higher temperature calcination if used as a structural promoter. The study completed x-ray diffraction spectroscopy and found little indication of change in crystal size in varying La promotion levels<sup>22</sup>. In comparison of non-promoted catalysts to La promoted catalysts, there is no indication of lanthanum crystallites in the XRD profile<sup>22</sup>. This suggests that the lanthanum is in highly dispersed form<sup>22</sup> and that it had little effect on the cobalt crystallite size. Using the Sherrer's equation, the crystalline size of Co<sub>3</sub>O<sub>4</sub> was calculated and it indicated that the

average particle size decreased with increasing lanthanum content, which results in a much higher dispersion<sup>22</sup>. The introduction of lanthanum on a titania supported cobalt catalyst could have a positive effect on the dispersion, which has been linked to the activity of the catalyst.

### 2.7.3 Zirconium Oxide (ZrO<sub>2</sub>)

A significant amount of research has been done in the addition of ZrO<sub>2</sub> to SiO<sub>2</sub> and TiO<sub>2</sub>, with little on the modification of Al<sub>2</sub>O<sub>3</sub>. The effect of zirconium modification to all supports seems to be controversial; however there is also differences in the preparation of these catalysts among authors. As previously discussed, it is difficult to separate the effect of preparation procedures, cobalt metal loading, and calcination temperatures to the zirconium loading effect.

Some research has shown higher activity and C<sub>5</sub>+ selectivity<sup>23</sup> in Fischer-Tropsch synthesis. Ali et al.<sup>24</sup> suggested that the promotion of zirconium on silica created an active interface with Co, which facilitates CO dissociation and thus increasing the activity. Rohr et al.<sup>25</sup> concluded that the modification of ZrO<sub>2</sub> on Co/Al<sub>2</sub>O<sub>3</sub> increased the activity and selectivity to heavier hydrocarbons, which was attributed to changes in surface coverage of reactive intermediates.

Some research has shown a weaker cobalt-zirconium interaction on Co/SiO<sub>2</sub> catalysts, which led to an increase in reducibility<sup>26</sup>. Other research indicates that there is no decrease in reduction for the addition of zirconia to Co/SiO<sub>2</sub> catalysts<sup>27</sup>. Moradi et al.<sup>23</sup> also found that the addition of zirconia to silica favors reduction at a

lower temperature concluding that the cobalt-silica interaction is replaced by the cobalt-zirconia interaction. The deposition of zirconia on silica support was proven to prevent the formation of cobalt silicate,<sup>27</sup> which also may mean that the cobalt-silica interaction is affected by the zirconia being present. Michalak et al, found that the addition of ZrO<sub>2</sub> had no impact on the surface area of the catalyst, but it decreased the extent of reduction for Co/Al<sub>2</sub>O<sub>3</sub> catalysts<sup>27</sup>. This may suggest that ZrO<sub>2</sub> inhibits the reduction of cobalt catalysts, supported on alumina.

XRD signals of both amorphous alumina and the addition of ZrO<sub>2</sub> to the alumina did not indicate any changes in signal, which leads us to believe that there was a strong interaction between ZrO<sub>2</sub> and the oxide composite.<sup>28</sup> This strong interaction likely resulted in highly dispersed ZrO<sub>2</sub> on alumina.

Xiong et al. synthesized ZrO<sub>2</sub>-Al<sub>2</sub>O<sub>3</sub> through impregnation of zirconium to a precalcined  $\gamma$ -Al<sub>2</sub>O<sub>3</sub> and found that the cobalt oxide crystallite size increased with increasing zirconium, while the zirconia inhibited formation of cobalt aluminate in those catalysts<sup>29</sup>. Xiong also found that an increase in zirconia decreased the methane selectivity, increased CO hydrogen activity, and C<sub>5</sub>+ selectivity in Fischer-Tropsch synthesis.

## 2.8 Brunauer Emmet Teller (BET) Surface Area Measurements

Brunauer, Emmet, Teller (BET)<sup>4</sup> surface area measurements are important for Fischer-Tropsch catalysts because the results provide surface area data, which are necessary to determine the available surface area for the reaction to take place.

The surface area of granulated powders is measured by determining the quantity of gas that adsorbs as a single layer of molecules, which is completed near the boiling point of the adsorbate gas. At the boiling point, the area covered by each gas molecule is known within minimal error and the sample surface area is calculated directly from the number of adsorbed molecules, the conditions, and the area occupied by each molecule. In most instances, 30% nitrogen in helium mixture is used at atmospheric pressure and at liquid nitrogen temperature. The adsorption of gas on a solid surface is described by the following equation<sup>4</sup> :

$$\left(\frac{P}{P_0}\right) \left(\frac{1}{V}\right) \left(1 - \frac{P}{P_0}\right) = \frac{1}{V_m C} + \frac{C - 1}{V_m C} \left(\frac{P}{P_0}\right)$$

*V = the volume of gas adsorbed at pressure P at standard temperature and pressure*  
*P<sub>0</sub> = the saturation pressure or vapor pressure of liquified gas at the absorbing temperature*  
*V<sub>m</sub> = the volume of gas (STP) required to form an adsorbed monomolecular layer*  
*C = a constant related to the energy of adsorption*

The surface area (S) of the sample is determined by the monolayer of adsorbed gas volume (V<sub>m</sub>) at standard temperature and pressure, given in the following equation:

$$S = \left(\frac{V_m A N}{M}\right)$$

*A = Avagadro's number*  
*M = molar volume of the gas*  
*N = the area of each adsorbed gas molecule*

Applicable BET surface area data and BJH adsorption data of Fischer-Tropsch cobalt catalysts available in literature is presented in Table 2.1. This data provides a

means for comparison of data collected in the work presented in this thesis to other literature available.

Table 2.1: BET Data from Literature

	BET Surface Area (m <sup>2</sup> /g)	Single Point adsorption average pore volume (cm <sup>3</sup> /g)	Single point adsorption average pore radius (nm)	Ref.
15%Co/Al <sub>2</sub> O <sub>3</sub>	144	0.38	5.25	29
15%Co/1%Zr/Al <sub>2</sub> O <sub>3</sub>	159	0.4	5.0	29
15%Co/5%Zr/Al <sub>2</sub> O <sub>3</sub>	133	0.35	5.2	29
15%Co/9%Zr/Al <sub>2</sub> O <sub>3</sub>	123	0.31	5.1	29
Al <sub>2</sub> O <sub>3</sub>	136			27
8.5%ZrO <sub>2</sub> /Al <sub>2</sub> O <sub>3</sub>	120			27
10%Co/Al <sub>2</sub> O <sub>3</sub>	103			27
10%Co/ZrO <sub>2</sub> /Al <sub>2</sub> O <sub>3</sub>	75			27
TiO <sub>2</sub>	49.5			27
8.5%ZrO <sub>2</sub> /TiO <sub>2</sub>	47.6			27
10%Co/TiO <sub>2</sub>	38.3			27
10%Co/ZrO <sub>2</sub> /TiO <sub>2</sub>	38.0			27

\*\*Blank spaces were left when data was unavailable

## 2.9 Temperature Programmed Reduction and Temperature Programmed Reduction After Reduction

Since Fischer-Tropsch cobalt catalysts oxidize readily in air, it is critical that the catalysts are reduced before introducing them to the reaction. If reduction is not completed at the optimum conditions, the catalyst may sinter and/or agglomerate during the process. Thermodynamics determine the best conditions at which a catalyst can be reduced, but are only useful if the catalyst particles are equivalent<sup>30</sup>, meaning that the cobalt particle sizes are uniform and is typically not the case with Fischer-Tropsch catalysts.

TPR provides useful information on the temperature that is needed for the complete reduction of the catalyst<sup>30</sup>. However, this temperature is often not the optimum condition for reduction, many other factors are considered for this determination. The area under the TPR curve represents the total hydrogen consumption and is commonly expressed in moles of H<sub>2</sub> consumer per mole of metal atoms (H<sub>2</sub>/M)<sup>30</sup>. Most frequently, TPR profiles are interpreted on a qualitative basis and not a quantitative.

During TPR, the metal oxide (cobalt oxide) reacts with hydrogen to form pure metal (cobalt metal). This reaction is also known as reduction. During the TPR, argon is used as the carrier gas because it has a very low relative thermal conductivity. The argon is blended in a fixed proportion with hydrogen, the reduction gas, which has a much higher thermal conductivity. The gas mixture flows through the analyzer, the sample, and then the detector. A baseline reading is established by the detector when the initial H<sub>2</sub>/Ar gas flows over the sample. This

occurs at a low enough temperature that no reduction has begun. As the temperature is increased at a fixed ramp rate, the hydrogen atoms begin to react with the sample. This reaction produces H<sub>2</sub>O molecules, which are removed from the gas stream using a cold trap. The production of H<sub>2</sub>O results in a decrease in the amount of hydrogen, thus shifting the total gas thermal conductivity towards the argon's thermal conductivity. As previously mentioned, argon has a lower thermal conductivity than hydrogen, so the total gas thermal conductivity decreases. The signal the instrument records is the electrical demand, also known as the detector signal. This demand is described as the amount of electricity it takes to keep the TCD at a constant filament temperature. So, as the total gas thermal conductivity decreases, the flowing gas removes heat from the filament more slowly, therefore it requires less electricity to maintain the filament temperature.

## 2.10 Hydrogen Chemisorption and Pulse Reoxidation

Hydrogen chemisorption and pulse reoxidation provide useful information about the catalyst's active site density, dispersion, cluster size, and reducibility. The hydrogen temperature programmed desorption (TPD) provides data on the active site density and is also used to calculate uncorrected dispersion. These calculations are done under the assumption that all of the cobalt was reduced and that one hydrogen atom attaches to one surface cobalt metal atom. Since it was not completely reduced, the use of pulse reoxidation becomes important. The pulse reoxidation data is used to calculate the extent of reduction, which is then used to determine the corrected dispersion and cluster size. The assumption in this

calculation is that for every two oxygen molecules consumed, there are three moles of bulk cobalt metal atoms previously reduced.

Table 2.2: Hydrogen Chemisorption Data from Literature

Catalyst Description	$\mu\text{moles H}_2$ desorbed per $\text{g}_{\text{cat}}$	Uncorrected Dispersion (%)	Uncorrected Diameter (nm)	$\mu\text{moles O}_2$ consumed per $\text{g}_{\text{cat}}$	% Reduction	Corrected Dispersion (%)	Corrected Diameter (nm)	Ref
10%Co-0%Mn-TiO2		7.16	11.8					31
10%Co-0.03%Mn-TiO2		6.03	9.7					31
10%Co-0.32%Mn-TiO2		7.16	10.4					31
10%Co-0.96%Mn-TiO2		2.50	9.2					31
10%Co-3.43%Mn-TiO2		1.77	9.6					31
15%Co-SiO2 CS		7.4			91.1		17.2	16
15%Co-TiO2/SiO2 CTSP		8.8			64.6		14.6	16

Catalyst Description	$\mu\text{moles H}_2$ desorbed per $\text{g}_{\text{cat}}$	Uncorrected Dispersion (%)	Uncorrected Diameter (nm)	$\mu\text{moles O}_2$ consumed per $\text{g}_{\text{cat}}$	% Reduction	Corrected Dispersion (%)	Corrected Diameter (nm)	Ref
15%Co- TiO2/SiO2 CTSI		8.7			69.9		14.7	16
15%Co- TiO2/SiO2 CTSHR		8.6			61.2		14.8	16
15%Co- TiO2/SiO2 CTSSG		10.2			35.4		12.6	16
12%Co-Ti-0La					81.66		15.7	22
12%Co-Ti-1/2000La					82.90		15.8	22
12%Co-Ti-1/200La					84.12		13.9	22
12%Co-Ti-1/120La					87.25		12.1	22
12%Co-Ti-1/20La					88.76		12.8	22
15%Co/Al <sub>2</sub> O <sub>3</sub>	88.4	6.94	14.9	898.4	52.68	13.2	7.9	29
15%Co/0.5%Zr/Al <sub>2</sub> O <sub>3</sub>	74.0	5.82	17.7	959.1	53.24	10.4	10.0	29
15%Co/1%Zr/Al <sub>2</sub> O <sub>3</sub>	74.2	5.83	17.5	910.2	53.37	10.9	9.3	29

Catalyst Description	$\mu\text{moles H}_2$ desorbed per $\text{g}_{\text{cat}}$	Uncorrected Dispersion (%)	Uncorrected Diameter (nm)	$\mu\text{moles O}_2$ consumed per $\text{g}_{\text{cat}}$	% Reduction	Corrected Dispersion (%)	Corrected Diameter (nm)	Ref
15%Co/5%Zr/Al <sub>2</sub> O <sub>3</sub>	102.5	8.05	12.8	855.8	50.18	16.0	6.4	29
15%Co/9%Zr/Al <sub>2</sub> O <sub>3</sub>	99.2	7.01	14.7	1005.8	58.95	11.9	8.7	29
15%Co/15%Zr/Al <sub>2</sub> O <sub>3</sub>	100.0	7.73	13.4	1020.4	59.91	15.1	8.0	29
10%Co/Al <sub>2</sub> O <sub>3</sub>		0.4			67		270	27
10%Co/8.5%ZrO <sub>2</sub> /Al <sub>2</sub> O <sub>3</sub>		1.1			61		101	27

\*\*Blank spaces were left when data was unavailable

## 2.11 X-ray Diffraction

X-ray diffraction provides a way to estimate the cobalt oxide crystallite size. Alumina is found at  $2\theta=45.66, 66.6^{29}$ . and spinel cobalt oxide is found at  $2\theta=31.3, 36.9, 45.1, 59.4, \text{ and } 65.4^{32}$ . Table 2.3 provides XRD data from literature for a baseline comparison to the data presented in this study.

Table 2.3: XRD Data from Literature

Catalyst	Average diameter of $\text{Co}_3\text{O}_4$ domains (nm)	Ref.
15%Co/ $\text{Al}_2\text{O}_3$	18.3	29
15%Co/0.5%Zr/ $\text{Al}_2\text{O}_3$	18.2	29
15%Co/1%Zr/ $\text{Al}_2\text{O}_3$	19.1	29
15%Co/5%Zr/ $\text{Al}_2\text{O}_3$	19.3	29
15%Co/9%Zr/ $\text{Al}_2\text{O}_3$	18.4	29
15%Co/15%Zr/ $\text{Al}_2\text{O}_3$	20.8	29

## CHAPTER III

### EXPERIMENTAL PROCEDURES

#### 3.1 Catalyst Preparation

In this study, Puralox SCFa-140/L3 (Sasol), Puralox SCFa-200Zr3 (Sasol), and Puralox TH 100/150 Ti10 (Sasol) were used as the explored catalyst supports. Puralox HP14/150 Al, Catalox Al<sub>2</sub>O<sub>3</sub> SBA200, and Catalox Al<sub>2</sub>O<sub>3</sub> SBA150 were used as the reference catalyst supports. These reference pairs were chosen because of their surface area and pore size data collected: 9.7%TiO<sub>2</sub>-Al<sub>2</sub>O<sub>3</sub> compared to both Al<sub>2</sub>O<sub>3</sub> SBA 150 and Al<sub>2</sub>O<sub>3</sub> HF14/150, 3.1%ZrO<sub>2</sub>-Al<sub>2</sub>O<sub>3</sub> compared to both Al<sub>2</sub>O<sub>3</sub> SBA 150 and Al<sub>2</sub>O<sub>3</sub> SBA 200, and 3.0%La<sub>2</sub>O<sub>3</sub>-Al<sub>2</sub>O<sub>3</sub> compared to both Al<sub>2</sub>O<sub>3</sub> SBA 150 and Al<sub>2</sub>O<sub>3</sub> SBA 200. All six supports are readily available for purchase from Sasol North America. Table 3.1 shows the composition, surface area, loose bulk density, and particle size distribution data provided by Sasol North America upon delivery of these supports.

Table 3.1: Catalyst support composition

Support Name	Composition	Surface Area (m <sup>2</sup> /g)	Loose Bulk Density (g/l)	Particle Size Distribution %	
Puralox TH 100/150 Ti10	90.3%Al <sub>2</sub> O <sub>3</sub> 9.7%TiO <sub>2</sub>	135	0.33	<25 μm	50.6
				<45 μm	82.5
				<90 μm	100
Puralox SCFa-140/L3 Lot No: BD2186	97% Al <sub>2</sub> O <sub>3</sub> 3%La <sub>2</sub> O <sub>3</sub>	143	0.61	<25 μm	33
				<45 μm	60
				<90 μm	94.7
				>150 μm	0.1
Puralox SCFa-200 Zr3 Lot No: BD2801	96.9%Al <sub>2</sub> O <sub>3</sub> 3.1%ZrO <sub>2</sub>	196	0.67	<25 μm	49.2
				<45 μm	82.1
				<90 μm	100
				>150 μm	0
Puralox HP14/150 Al	100%Al <sub>2</sub> O <sub>3</sub>	150			
Catalox Al <sub>2</sub> O <sub>3</sub> SBA200	100%Al <sub>2</sub> O <sub>3</sub>	200			
Catalox Al <sub>2</sub> O <sub>3</sub> SBA150	100%Al <sub>2</sub> O <sub>3</sub>	150			

Support calcination is necessary to drive off any water that may be absorbed on the support from the atmosphere. The support calcinations were carried out using a tubular reactor and a clamshell furnace. A Lindberg/Blue M control console was used to set the parameters of the experiment and control the internal temperature of the support throughout the calcination procedure.

For all three catalyst supports, approximately 30 grams were loaded into the reactor. The reactor was then loaded into the furnace, and the air supply turned on at a flow rate of approximately 2.0 L/min set on a rotameter. The source of the air used in the experiment was a gas cylinder of zero air. The controller was set to ramp at 2°C/min from room temperature to 400°C and then it was held at 400°C for four hours. The sample was then kept under air flow until reaching room temperature and then removed from the tubular reactor and stored in an oven at 100°C until the first cobalt loading began. Figure 3.1 shows the diagram of the calcination reactor, a plug flow reactor (PFR). The air flows from the top of the reactor over the catalyst bed and out the bottom of the reactor, with a thermocouple located in the middle of the catalyst bed.

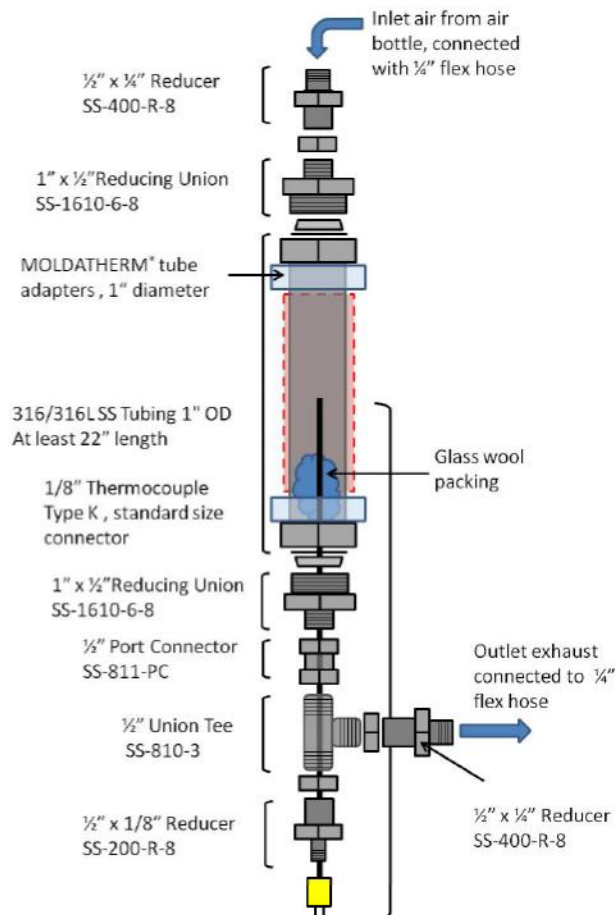


Figure 3.1: Calcination reactor drawing

Impregnation is one of the many different methods for synthesizing Fischer-Tropsch (F-T) catalysts, which can be done through incipient wetness impregnation (IWI) or slurry impregnation. Incipient wetness impregnation uses a loading solution that is equal to the exact volume of pores in the support, while slurry impregnation requires the final loading solution to be equal to 2.5 times the total pore volume of the support. Previous research has shown that incipient wetness impregnation procedures have been found to produce a wider range of cluster sizes than the slurry phase impregnation procedure<sup>7</sup>. Because of the wide range of

cluster sizes in IWI procedures, slurry phase impregnation was chosen for this study.

The catalyst was prepared using slurry impregnation and two separate loadings of cobalt were made using cobalt nitrate and water. The first loading required half of the cobalt nitrate needed for 15% by weight loading. This cobalt nitrate was dissolved in de-ionized water so that the total volume was equivalent to 2.5 times the total pore volume for the specified support. The solution was then added (drop wise via a burette and a rotating round bottom flask) to the catalyst support until approximately  $\frac{1}{4}$  of the solution was dispensed. At this time, the round bottom flask was removed from the rotating mechanism and thoroughly mixed by shaking and scraping the walls of the round bottom flask. This process was continued until the entire solution was added to the support. The round bottom flask was then transferred to the rotary evaporator where the vacuum was controlled to ensure very slow drying of the catalyst. The second loading of cobalt was completed using the same methods.

After completion of both cobalt nitrate loadings, the nitrate must be driven off through catalyst calcination. This calcination was completed using the same furnace and control system previously mentioned in the support calcination description; however a separate tubular reactor was used to avoid contamination. Zero air flow was set to approximately 2L/min and the temperature controller was set to ramp up at a rate of 2°C/min from room temperature to 350°C and hold at 350°C for 4 hours. After completion of calcination, the air flow was maintained until proper cool down of the catalyst.

## 3.2 Catalyst Characterization

A number of catalyst characterization techniques were used including: Scanning electron microscopy (SEM) and electron dispersed spectroscopy(EDS), Brunauer Emmet Teller (BET), Barrett Joyner Halenda (BJH), temperature programmed reduction (TPR), temperature programmed reduction after reduction (TPR-AR), hydrogen chemisorption with pulse reoxidation, and x-ray diffraction (XRD).

### 3.2.1 Scanning Electron Microscopy and Electron Dispersed Spectroscopy

Scanning electron microscopy (SEM) images were gathered on only doped alumina supports using a Hitachi S-3000N equipped with an EDAX detector for electron dispersed spectroscopy (EDS) measurements. The SEM was set to 25kV for imaging and the EDAX working distance was set to 15mm before measurements were taken. SEM-EDS measurements were gathered on each of the doped alumina supports in order to better understand the surface morphology of the dopants. The samples were prepared and mounted on copper tape before measurements were taken.

### 3.2.2 Brunauer Emmet Teller (BET) Surface Area Measurements and Barrett Joyner Halenda (BJH) Pore Size Distributions

BET (Brunauer, Emmet, and Teller<sup>4</sup>) and BJH (Barrett Joyner Halenda <sup>33</sup>) measurements were conducted on all of the supports, as well as the catalysts to determine the loss of surface area after loading cobalt metal. These measurements were conducted using a Micromeritics Tri-Star system. Approximately 0.5 grams of sample was prepared by slowly ramping to 160°C and evacuating to 50mTorr. This preparation step was completed in order to remove any water or other contaminants on the surface of the catalyst or support. The BET surface area measurements were completed with nitrogen and argon as the adsorption gases.

### 3.2.3 Temperature Programmed Reduction (TPR)

Temperature programmed reduction (TPR) profiles were obtained for each of the calcined catalysts using a Zeton Altamira AMI-200 unit. Each sample was loaded into a Zeton Altamira sample tube with a target mass of 0.1 grams. The sample tubes were installed on the instrument and then set to undergo argon pretreatment. The samples were heated to 350°C at a rate of 10°C/min under argon flow of 30cm<sup>3</sup>/min in order to remove any residual water or nitrate. After argon pretreatment, the sample was cooled to 50°C and held under continuous flow of argon for 15 minutes. The flow was then switched from pure argon to 10% hydrogen in argon (remaining at a constant 30 cm<sup>3</sup>/min). At this point the TCD

signal started recording and the ramp rate was set to 10°C/min from 50°C to 1100°C and the sample was held at 1100°C for a minimum of 30 minutes.

### 3.2.4 Temperature Programmed Reduction After Reduction

Temperature programmed reduction after reduction (TPR-AR) profiles were obtained for all of the calcined catalysts using a Zeton-Altamira AMI-200 unit. The first step was argon pretreatment step, which was mentioned previously in the TPR section. After argon pretreatment, the sample was reduced under 30cm<sup>3</sup>/min flow of 33% hydrogen in argon at a ramp rate of 1°C/min from room temperature up to 350°C and held for 10 hours. The flow was then switched to 10% hydrogen in argon and the TCD began recording. The sample was then heated to 1100°C at a ramp rate of 10°C/min.

### 3.2.5 Hydrogen Chemisorption with Pulse Reoxidation

Hydrogen chemisorption with pulse reoxidation measurements were performed on the calcined catalysts using a Zeton Altamira AMI-200 unit, which incorporates a thermal conductivity detector. Each sample weight was approximately 0.22 grams. The catalyst was loaded via a sample tube and activated at 350°C for 10 hours using a flow of 33% hydrogen in argon and then cooled under hydrogen flow to 100°C. The sample was held at 100°C, while switching the flow to pure argon in order to prevent physisorption of weakly bound species. The sample was then slowly increased to activation temperature and held under flowing argon

to desorb the remaining chemisorbed hydrogen and the TCD signal returned to baseline. This TPD spectrum was integrated in order to find the number of hydrogen moles desorbed in comparison to the area of the calibrated hydrogen pulse's peaks. The hydrogen TPD results are then used for calculating uncorrected dispersion.

The same sample was reoxidized by injecting pulses of pure oxygen in helium in reference to pure helium gas at the activation temperature. The number of moles of oxygen consumed by the sample was determined by integration of the peaks and using the same calibration method for hydrogen chemisorption. Assuming that all of the  $\text{Co}^0$  reoxidized to  $\text{Co}_3\text{O}_4$ , the percentage reduction was calculated. The uncorrected dispersions are based on the assumption of complete reduction, where the corrected dispersions include the percentage of reduced cobalt. The number of  $\text{Co}^0$  moles on the surface is determined by the number of hydrogen desorbed during TPD and the total number of moles of  $\text{Co}^0$  in the sample is the preparation target weight percent of cobalt.

### 3.2.6 X-ray Diffraction

X-ray diffraction profiles were obtained for each of the calcined catalyst using a Philips X'Pert unit. A long range scan was ran from 15 to 80° with 0.02° steps at 5 seconds/step. In order to quantify the average  $\text{Co}_3\text{O}_4$  cluster sizes using the Scherrer equation at  $2\theta=36.8^\circ$ , which represents (3 1 1), a shorter range scan was

also made. The shorter scan range was from 30 to 45° with 0.01° steps at 15 seconds/step.

## CHAPTER IV

### CATALYST CHARACTERIZATION RESULTS

#### 4.1 Scanning Electron Microscopy and Electron Dispersed Spectroscopy

Figure 4.1 shows the scanning electron microscopy-energy dispersive spectroscopy (SEM-EDS) mapping results for both alumina and titanium for the 9.7%TiO<sub>2</sub>-Al<sub>2</sub>O<sub>3</sub> support. The left image highlights the alumina in pink and the right image highlights the titanium in green. The alumina appears to be the stronger presence and highlights the particles shapes because of the concentration of alumina being detected by SEM-EDS. The titanium appears to be highly dispersed and have less concentration on the sample. This relationship was expected as the 9.7%TiO<sub>2</sub>-Al<sub>2</sub>O<sub>3</sub> support contains less than 10% titanium. Since SEM-EDS has a penetration of approximately 2μm, it is likely that most of the titanium is on or near the surface of the support, which make it available to contribute to the F-T reaction.

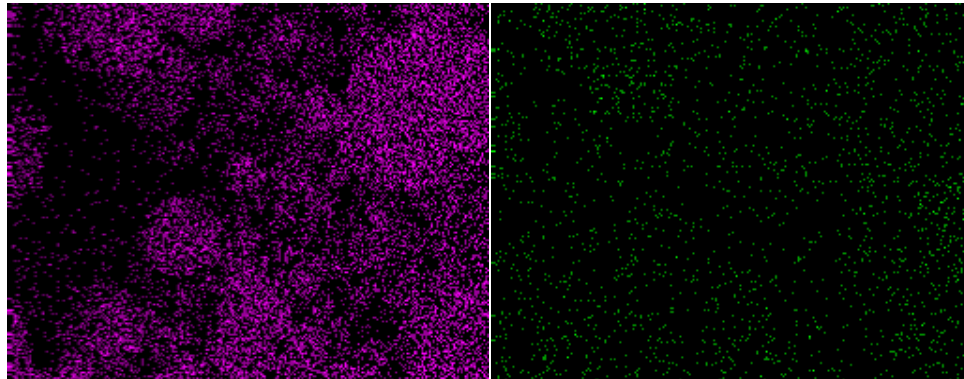


Figure 4.1: Scanning Electron Microscopy-Energy Dispersive Spectroscopy (SEM-EDS) mapping results for 9.7%TiO<sub>2</sub>-Al<sub>2</sub>O<sub>3</sub> where Al<sub>2</sub>O<sub>3</sub> is pink (left) and TiO<sub>2</sub> is green (right).

Figure 4.2 shows the overlay of the SEM-EDS mapping results for both alumina and titanium separately on the actual SEM image of the 9.7%TiO<sub>2</sub>-Al<sub>2</sub>O<sub>3</sub> support. The left image highlights the alumina only (in pink) and the right image highlights the titanium only (in green). As previously discussed, the alumina shows a higher concentration and highlights the support particles structure because of this higher concentration. The titanium appears to be uniformly dispersed over all support particles in this image.

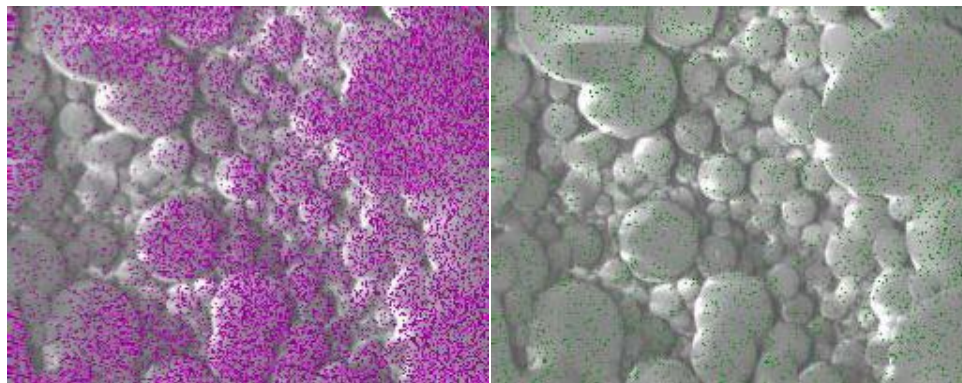


Figure 4.2: Scanning Electron Microscopy-Energy Dispersive Spectroscopy (SEM-EDS) mapping results overlaid on scanning electron microscopy image for 9.7%TiO<sub>2</sub>-Al<sub>2</sub>O<sub>3</sub> where Al<sub>2</sub>O<sub>3</sub> is pink (left) and TiO<sub>2</sub> is green (right).

Figure 4.3 shows the overlay of both alumina and titanium SEM-EDS mapping results on top of the actual SEM image of the 9.7%TiO<sub>2</sub>-Al<sub>2</sub>O<sub>3</sub> support. This image puts previous conclusions into perspective. It is difficult to see the titanium among the alumina mapping results, likely because of the highly dispersed titanium on the surface.

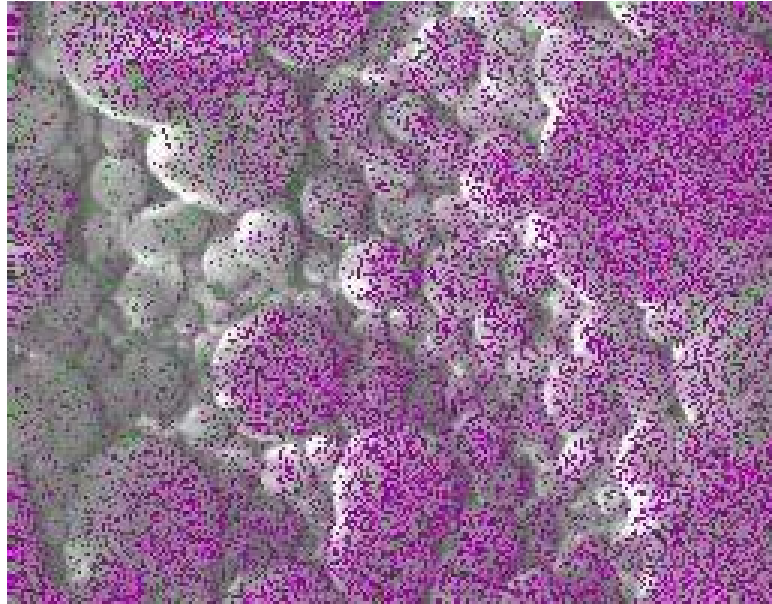


Figure 4.3: Scanning Electron Microscopy-Energy Dispersive Spectroscopy (SEM-EDS) mapping results for 9.7%TiO<sub>2</sub>-Al<sub>2</sub>O<sub>3</sub> overlaid on scanning electron microscopy image. Alumina is highlighted in pink and titania is highlighted in green.

Figure 4.4 and Table 4.1 show the SEM-EDS quantitative results for 9.7%TiO<sub>2</sub>-Al<sub>2</sub>O<sub>3</sub>. Figure 4.4 shows three distinct peaks: alumina, titanium, and the copper tape used to mount the sample. Results indicate an atomic % of titanium as 8.17%, which is in order with the expected 9.7% of titanium.

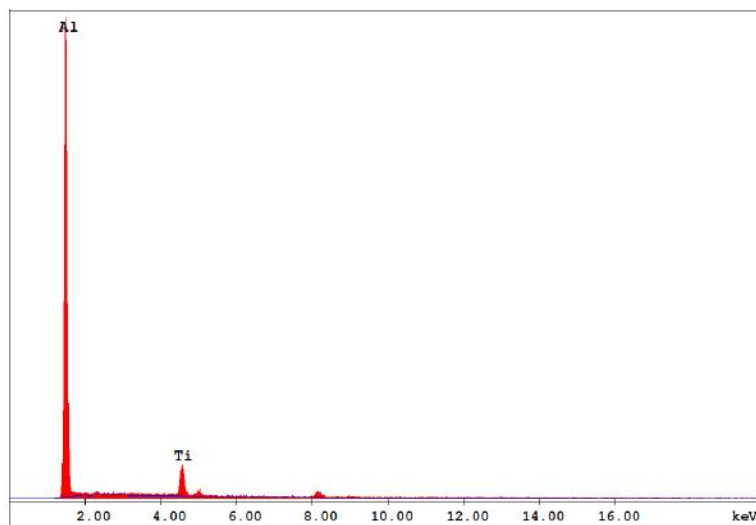


Figure 4.4: Scanning Electron Microscopy-Energy Dispersive Spectroscopy (SEM-EDS) quantitative results for 9.7%TiO<sub>2</sub>-Al<sub>2</sub>O<sub>3</sub> support.

Table 4.1: Scanning Electron Microscopy-Energy Dispersive Spectroscopy (SEM-EDS) quantitative results for 9.7%TiO<sub>2</sub>-Al<sub>2</sub>O<sub>3</sub>

Element	Wt%	At%	K-Ratio	Z	A	F
AlK	86.35	91.83	0.7122	1.01	0.8162	1.0006
TiK	13.65	8.17	0.1128	0.9282	0.8904	1.0000

Figure 4.5 shows the scanning electron microscopy-energy dispersive spectroscopy (SEM-EDS) mapping results for both alumina and lanthanum for the 3.0%La<sub>2</sub>O<sub>3</sub>-Al<sub>2</sub>O<sub>3</sub> support. The left image highlights the alumina in pink and the right image highlights the lanthanum in green. Again, alumina appears to be the stronger presence and highlights the particles shapes because of the concentration of alumina being detected by SEM-EDS. The lanthanum appears to be highly dispersed and have less concentration on the sample, even less than the previously discussed titanium. This relationship was expected as the 3.0%La<sub>2</sub>O<sub>3</sub>-Al<sub>2</sub>O<sub>3</sub> support

contains only 3% lanthanum. Since SEM-EDS has a penetration of approximately  $2\mu\text{m}$ , it is likely that most of the lanthanum is on or near the surface of the support.

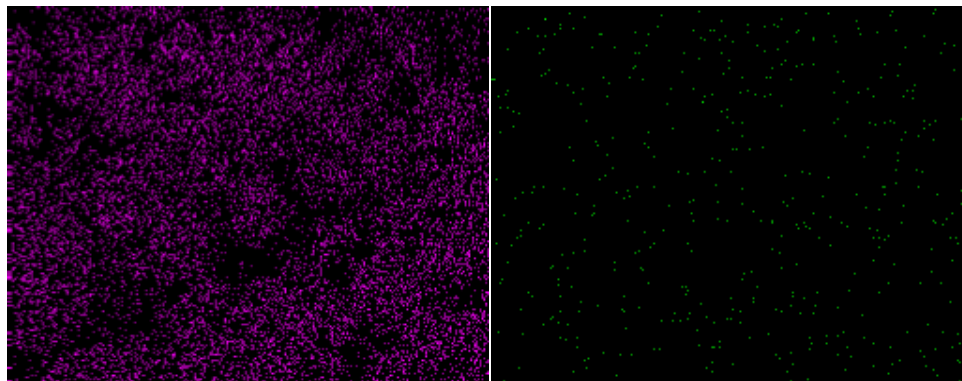


Figure 4.5: Scanning Electron Microscopy-Energy Dispersive Spectroscopy (SEM-EDS) mapping results for 3.0%La<sub>2</sub>O<sub>3</sub>-Al<sub>2</sub>O<sub>3</sub> where Al<sub>2</sub>O<sub>3</sub> is pink (left) and La<sub>2</sub>O<sub>3</sub> is green (right)..

Figure 4.6 shows the SEM-EDS mapping results overlaid on the SEM image for the 3.0%La<sub>2</sub>O<sub>3</sub>-Al<sub>2</sub>O<sub>3</sub> support. The alumina is highlighted in pink on the left image and shows the formation of the support particles. The lanthanum is shown highlighted in green on the right and appears to have a high dispersion.

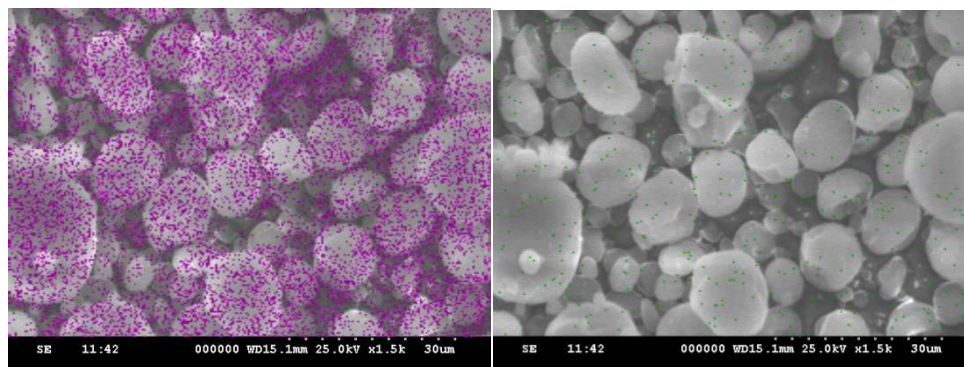


Figure 4.6: Scanning Electron Microscopy-Energy Dispersive Spectroscopy (SEM-EDS) mapping results overlaid on scanning electron microscopy image for 3.0%La<sub>2</sub>O<sub>3</sub>-Al<sub>2</sub>O<sub>3</sub> where Al<sub>2</sub>O<sub>3</sub> is pink (left) and La<sub>2</sub>O<sub>3</sub> is green (right).

Figure 4.8 shows the SEM-EDS mapping of both alumina and lanthanum overlaid on the SEM image. Similar to the titanium doped catalyst, the lanthanum is difficult to see and is likely well dispersed throughout the alumina. It is highly likely that the lanthanum is on or near the surface of the support and will play a role in the catalytic reaction.

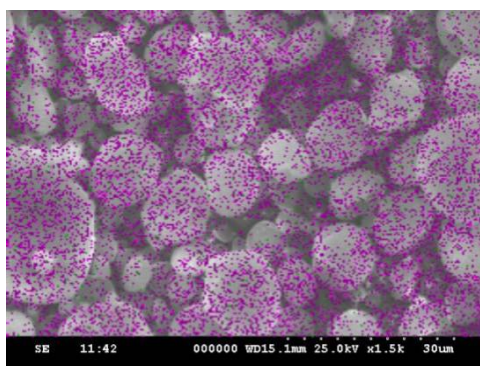


Figure 4.7: Scanning Electron Microscopy-Energy Dispersive Spectroscopy (SEM-EDS) mapping results for 3.0%La<sub>2</sub>O<sub>3</sub>-Al<sub>2</sub>O<sub>3</sub> overlaid on scanning electron microscopy image (Al<sub>2</sub>O<sub>3</sub> in pink and La<sub>2</sub>O<sub>3</sub> in green).

Figure 4.8: and Table 4.2 show the SEM-EDS quantitative results for the 3.0%La<sub>2</sub>O<sub>3</sub>-Al<sub>2</sub>O<sub>3</sub> support. The figure displays peaks relating to alumina, lanthanum and the copper tape used in mounting the sample. The quantitative results indicate 1.59% lanthanum, which is well within experimental error for the expected value of 3% lanthanum.

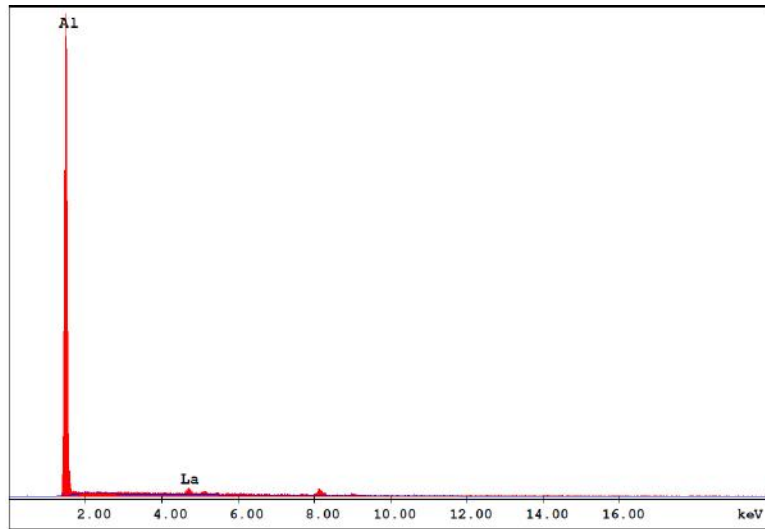


Figure 4.8: Scanning Electron Microscopy-Energy Dispersive Spectroscopy (SEM-EDS) quantitative results for 3.0%La<sub>2</sub>O<sub>3</sub>-Al<sub>2</sub>O<sub>3</sub>.

Table 4.2 Scanning Electron Microscopy-Energy Dispersive Spectroscopy (SEM-EDS) quantitative results for 3.0%La<sub>2</sub>O<sub>3</sub>-Al<sub>2</sub>O<sub>3</sub>.

Element	Wt%	At%	K-Ratio	Z	A	F
AlK	92.33	98.41	0.7041	1.0116	0.7537	1.0002
LaL	7.67	1.59	0.0636	0.8007	1.0346	1.0000

Figure 4.9: Scanning Electron Microscopy-Energy Dispersive Spectroscopy (SEM-EDS) mapping results for alumina highlighted in pink (left) and zirconium highlighted in green (right) on the 3.1%ZrO<sub>2</sub>-Al<sub>2</sub>O<sub>3</sub> support. Figure 4.9

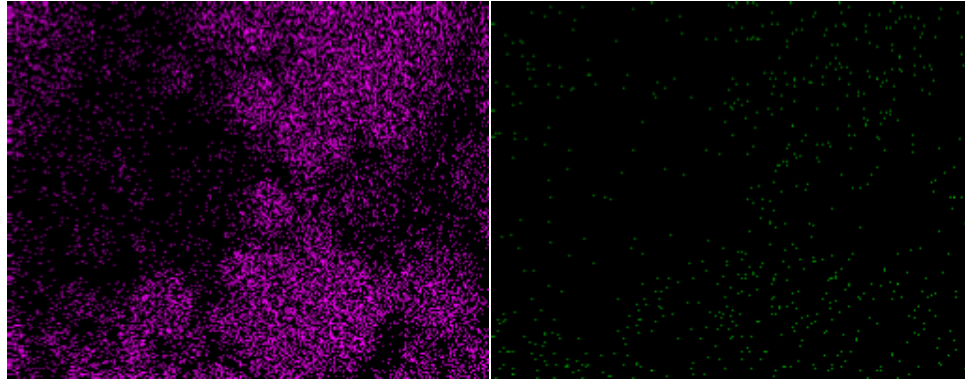


Figure 4.9: Scanning Electron Microscopy-Energy Dispersive Spectroscopy (SEM-EDS) mapping results for 3.1%ZrO<sub>2</sub>-Al<sub>2</sub>O<sub>3</sub> where Al<sub>2</sub>O<sub>3</sub> is pink (left) and ZrO<sub>2</sub> is green (right).

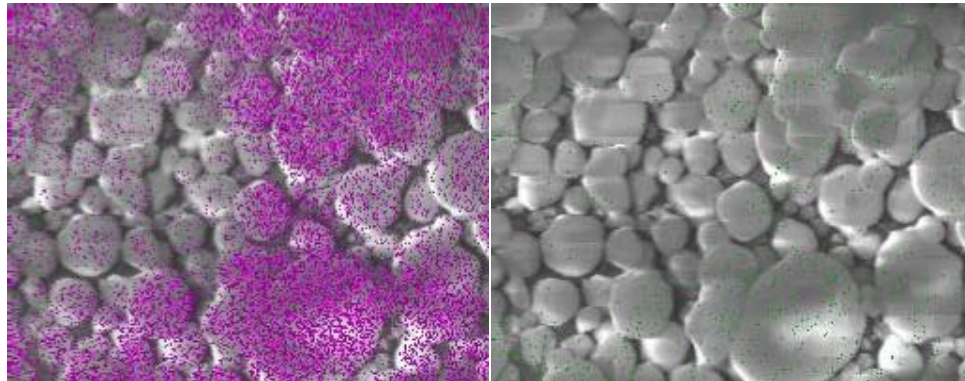


Figure 4.10: Scanning Electron Microscopy-Energy Dispersive Spectroscopy (SEM-EDS) mapping results overlaid on scanning electron microscopy image for 3.1%ZrO<sub>2</sub>-Al<sub>2</sub>O<sub>3</sub> where Al<sub>2</sub>O<sub>3</sub> is pink (left) and ZrO<sub>2</sub> is green (right).

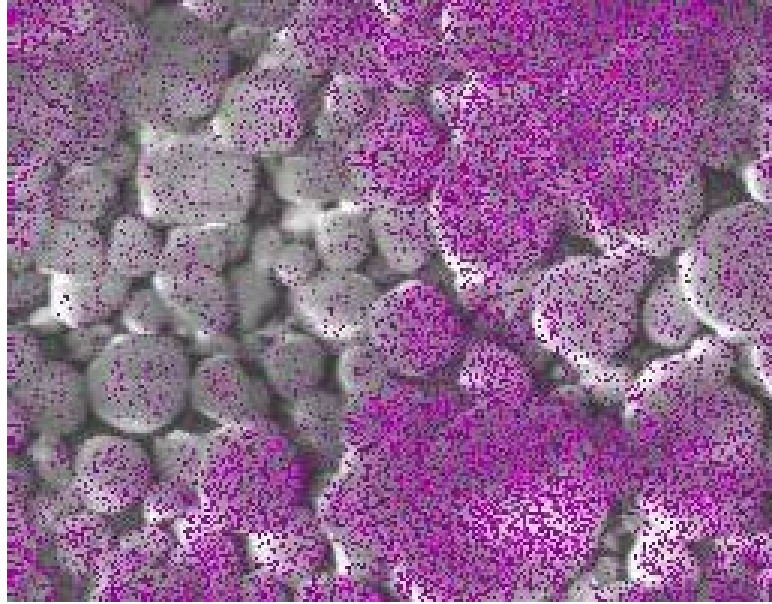


Figure 4.11: Scanning Electron Microscopy-Energy Dispersive Spectroscopy (SEM-EDS) mapping results for 3.1%ZrO<sub>2</sub>-Al<sub>2</sub>O<sub>3</sub> overlaid on scanning electron microscopy image where Al<sub>2</sub>O<sub>3</sub> is pink (left) and ZrO<sub>2</sub> is green (right).

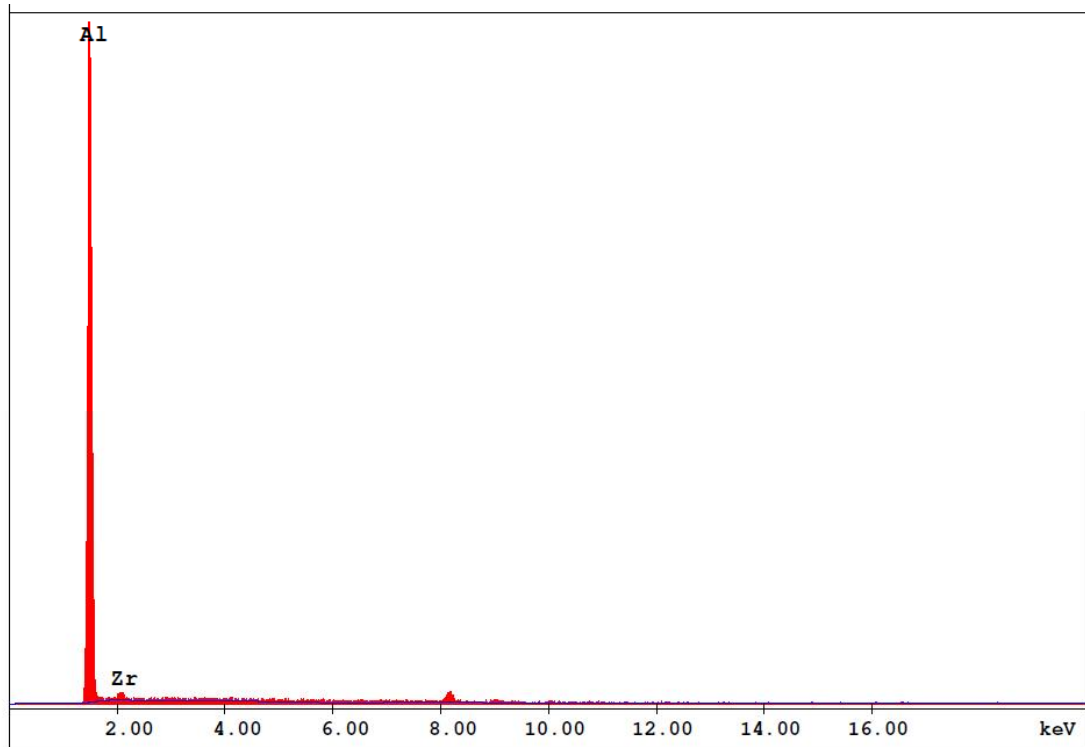


Figure 4.12: Scanning Electron Microscopy-Energy Dispersive Spectroscopy (SEM-EDS) quantitative results for 3.1%ZrO<sub>2</sub>-Al<sub>2</sub>O<sub>3</sub>

Table 4.3: Scanning Electron Microscopy-Energy Dispersive Spectroscopy (SEM-EDS) quantitative results for 3.1%ZrO<sub>2</sub>-Al<sub>2</sub>O<sub>3</sub>.

Element	Wt%	At%	K-Ratio	Z	A	F
AlK	91.23	97.23	0.8451	1.0104	0.9157	1.0013
ZrL	8.77	2.77	0.0336	0.8724	0.4387	1.0000

#### 4.2 Brunauer Emmet Teller (BET)<sup>4</sup> and Barrett Joyner Halenda (BJH)<sup>33</sup> Measurements

Surface area measurement by nitrogen adsorption and desorption results are shown in Table 4.4. The surface areas and average adsorption pore radii of Puralox TH 100/150 Ti<sub>10</sub>, Puralox SCFa-200 Zr<sub>3</sub>, and Puralox SCFa-140/L3 supports were measured to be 137.94 m<sup>2</sup>/g and 13.327 nm, 152.63 m<sup>2</sup>/g and 3.74 nm, and 142.26 m<sup>2</sup>/g and 6.27 nm respectively. The baseline support surface areas can be used to calculate the expected surface area of each support after the cobalt was loaded. Since BET was completed on the catalysts before reduction, the surface areas take into account cobalt oxide not cobalt metal. In order to determine potential pore blockage on the surface, the catalyst cobalt weight percents must be corrected to cobalt oxide weight percents. A weight percent of 15% cobalt metal is equivalent to 20% cobalt oxide (Co<sub>3</sub>O<sub>4</sub>). If we assume that the support is the only contributor to area, then the area of 15%Co/9.7%TiO<sub>2</sub>-Al<sub>2</sub>O<sub>3</sub> would be expected to be 0.80 x 137.94m<sup>2</sup>/g (the area of 9.7%TiO<sub>2</sub>-Al<sub>2</sub>O<sub>3</sub>)= 110.35 m<sup>2</sup>/g, which is within experimental error of the measured surface area of 113.26 m<sup>2</sup>/g. Similarly, the area of 15%Co/3.0%La<sub>2</sub>O<sub>3</sub>-Al<sub>2</sub>O<sub>3</sub> should be 0.8 x 142.26 m<sup>2</sup>/g (the surface area of 3.0%La<sub>2</sub>O<sub>3</sub>-Al<sub>2</sub>O<sub>3</sub>) = 113.81 m<sup>2</sup>/g, which also corresponds to the measured surface area of 124.41 m<sup>2</sup>/g quite well. Likewise, the area of 15%Co/3.1%ZrO<sub>2</sub>-Al<sub>2</sub>O<sub>3</sub> should be 0.8 x 183.5 m<sup>2</sup>/g (the area of 3.1%ZrO<sub>2</sub>-Al<sub>2</sub>O<sub>3</sub>)=146.8 m<sup>2</sup>/g, which matches the measured surface area of 152.63 m<sup>2</sup>/g reasonably well. These results can be compared more clearly in Figure 4.13.

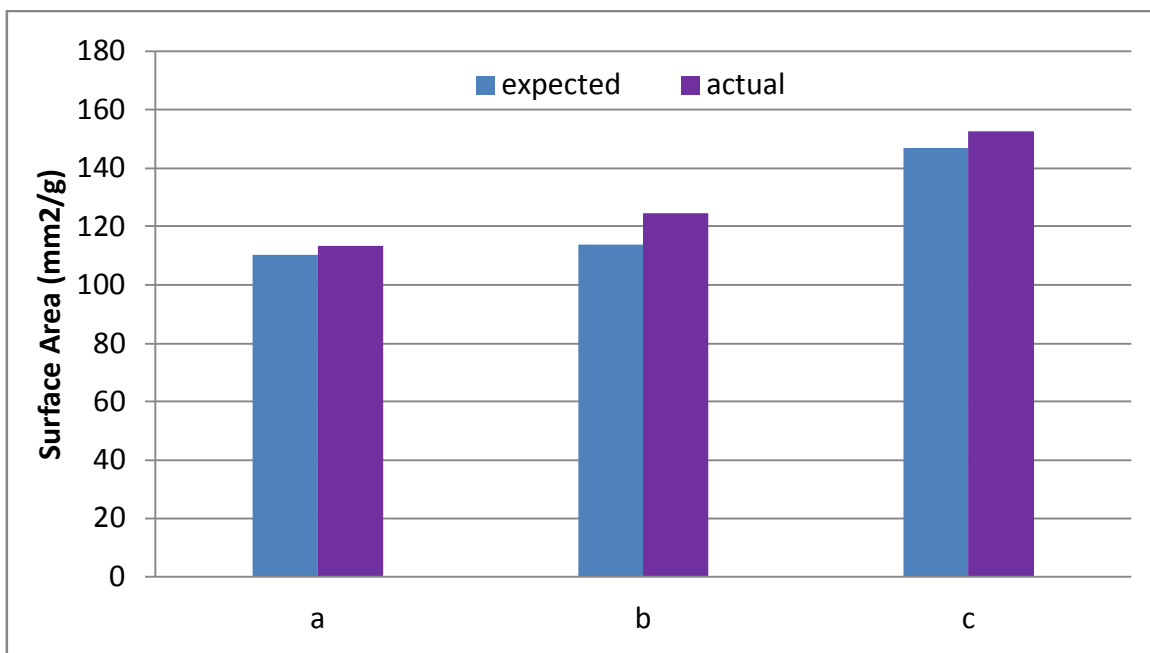


Figure 4.13: Expected BET surface areas of (a) 15%Co/9.7%TiO<sub>2</sub>-Al<sub>2</sub>O<sub>3</sub>, (b) 15%Co/3.0%La<sub>2</sub>O<sub>3</sub>-Al<sub>2</sub>O<sub>3</sub>, (c) 15%Co/3.1%ZrO<sub>2</sub>-Al<sub>2</sub>O<sub>3</sub>

The BET surface area results of the supports and their corresponding catalysts are shown in Figure 4.14. The surface area of the catalyst in relation to its bare support was expected to be lower, which was shown to be true for all supports upon addition of cobalt.

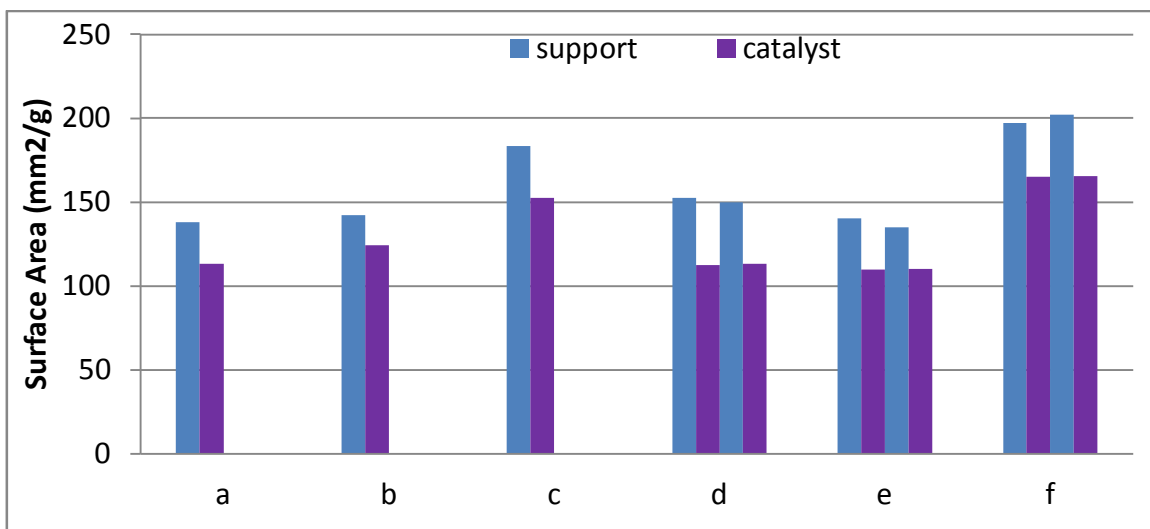


Figure 4.14: BET surface area comparison of (a) 15%Co/9.7%TiO<sub>2</sub>-Al<sub>2</sub>O<sub>3</sub>, (b) 15%Co/3.0%La<sub>2</sub>O<sub>3</sub>-Al<sub>2</sub>O<sub>3</sub>, (c) 15%Co/3.1%ZrO<sub>2</sub>-Al<sub>2</sub>O<sub>3</sub>, (d) 15%Co/Al<sub>2</sub>O<sub>3</sub> HP14/150, (e) 15%Co/Al<sub>2</sub>O<sub>3</sub> SBA150, and (f) 15%Co/Al<sub>2</sub>O<sub>3</sub> SBA200.

Along with surface area measurements, Table 4.4 also displays the BJH adsorption average pore radius. The BJH adsorption average pore radius data is also displayed in Figure 4.15 and the BJH desorption average pore volume is shown in Figure 4.16. In comparing each adsorption average pore radius, the cobalt loading decreased the pore radius on all three supports. The most significant reduction in pore radius was seen in the loading of 15% cobalt on the 9.7%TiO<sub>2</sub>-Al<sub>2</sub>O<sub>3</sub> support, where the support and catalyst pore radii were measured to be 13.37 nm and 10.92 nm respectively, which also had the largest pore radius. Since the pore radius decreased upon addition of cobalt to all of the supports, the data suggests that the pores were filled uniformly. The pore volume decreased slightly upon addition of cobalt to the support, as expected.

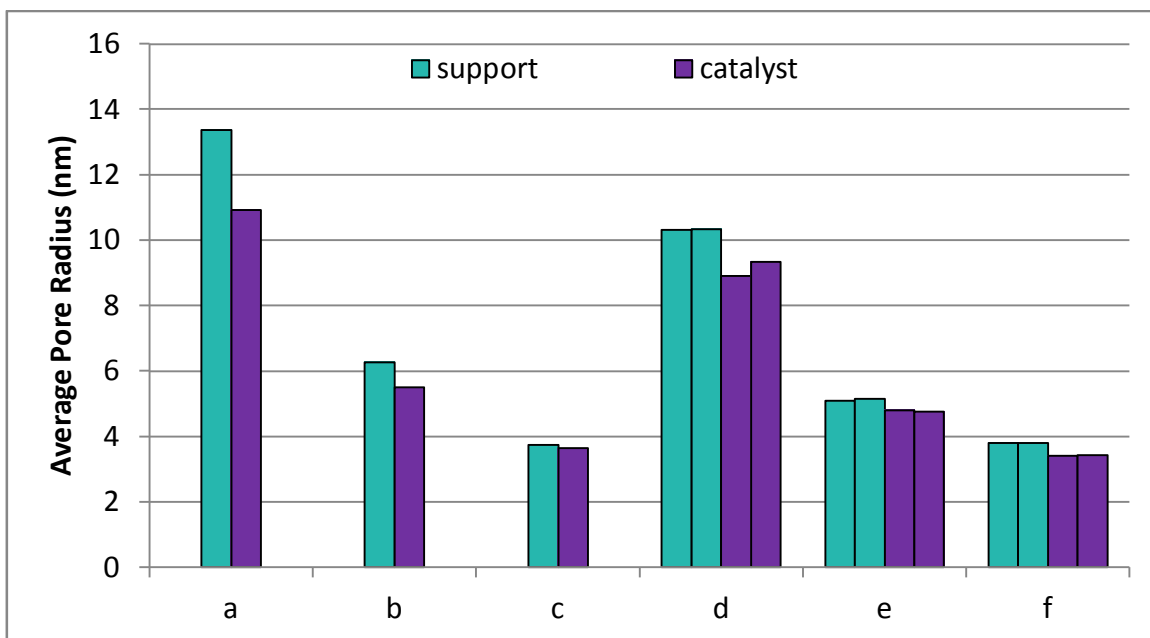


Figure 4.15: Barrett Joyner Halenda (BJH) average pore radius adsorption data for (a) 15%Co/9.7%TiO<sub>2</sub>-Al<sub>2</sub>O<sub>3</sub>, (b) 15%Co/3.0%La<sub>2</sub>O<sub>3</sub>-Al<sub>2</sub>O<sub>3</sub>, (c) 15%Co/3.1%ZrO<sub>2</sub>-Al<sub>2</sub>O<sub>3</sub>, (d) 15%Co/Al<sub>2</sub>O<sub>3</sub> HP14/150, (e) 15%Co/Al<sub>2</sub>O<sub>3</sub> SBA150, and (f) 15%Co/Al<sub>2</sub>O<sub>3</sub> SBA200.

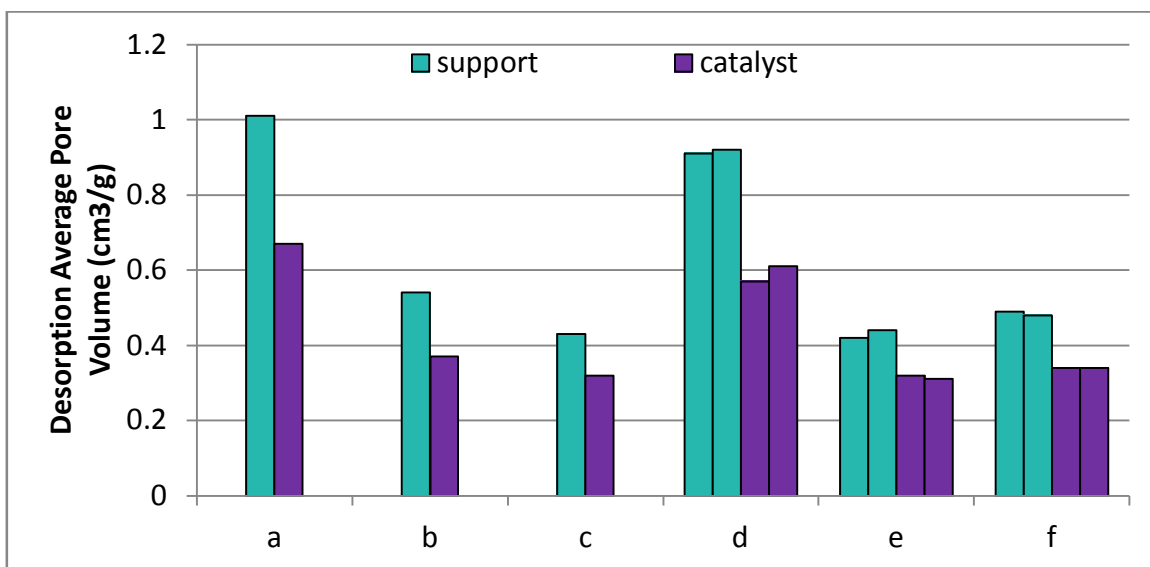


Figure 4.16: Barrett Joyner Halenda (BJH) average pore volume desorption data for (a) 15%Co/9.7%TiO<sub>2</sub>-Al<sub>2</sub>O<sub>3</sub>, (b) 15%Co/3.0%La<sub>2</sub>O<sub>3</sub>-Al<sub>2</sub>O<sub>3</sub>, (c) 15%Co/3.1%ZrO<sub>2</sub>-Al<sub>2</sub>O<sub>3</sub>, (d) 15%Co/Al<sub>2</sub>O<sub>3</sub> HP14/150, (e) 15%Co/Al<sub>2</sub>O<sub>3</sub> SBA150, and (f) 15%Co/Al<sub>2</sub>O<sub>3</sub> SBA200.

Table 4.4: BET surface area measurements and BJH pore volume and pore radius measurements

	BET Surface Area (m <sup>2</sup> /g)	Single Point adsorption average pore volume (cm <sup>3</sup> /g)	BJH adsorption/desorption average pore volume (cm <sup>3</sup> /g)	Single point adsorption average pore radius (nm)	BJH adsorption/desorption average pore radius (nm)
9.7%TiO <sub>2</sub> -Al <sub>2</sub> O <sub>3</sub>	137.9	1.012	1.01/1.01	---	13.37/11.10
15%Co/9.7%TiO <sub>2</sub> -Al <sub>2</sub> O <sub>3</sub>	113.3	0.6634	0.67/0.67	12.18	10.92/9.99
3.0%La <sub>2</sub> O <sub>3</sub> -Al <sub>2</sub> O <sub>3</sub>	142.26	0.5310	0.54/0.54	7.47	6.27/5.43
15%Co/3.0%La <sub>2</sub> O <sub>3</sub> -Al <sub>2</sub> O <sub>3</sub>	124.41	0.3681	0.37/0.37	6.14	5.49/5.05
3.1%ZrO <sub>2</sub> -Al <sub>2</sub> O <sub>3</sub>	183.5	0.4291	0.44/0.43	4.68	3.74/3.29
15%Co/3.1%ZrO <sub>2</sub> -Al <sub>2</sub> O <sub>3</sub>	152.63	0.3180	0.32/0.32	4.17	3.64/3.31
HP14/150 Al	152.6	0.9185	0.92/0.92	12.55	10.33/9.02
	149.8	0.9003	0.91/0.91	12.53	10.31/9.03
15%Co/Al <sub>2</sub> O <sub>3</sub> HP14/150	112.5	0.5320	0.57/0.57	9.46	8.90/8.12
	113.4	0.5728	0.60/0.61	10.09	9.34/8.38
Al <sub>2</sub> O <sub>3</sub> SBA150	140.2	0.4357	0.44/0.44	6.47	5.14/4.50
	135.1	0.4190	0.42/0.42	6.46	5.08/4.45
15%Co/Al <sub>2</sub> O <sub>3</sub> SBA150	109.8	0.3103	0.32/0.32	5.65	4.80/4.31
	110.2	0.3051	0.31/0.31	5.54	4.76/4.30
Al <sub>2</sub> O <sub>3</sub> SBA200	197.0	0.4730	0.48/0.48	5.00	3.79/3.37
	202.2	0.4847	0.49/0.49	5.00	3.80/3.36
15%Co/Al <sub>2</sub> O <sub>3</sub> SBA200	165.0	0.3351	0.34/0.34	4.06	3.41/3.09
	165.4	0.3375	0.34/0.34	4.08	3.42/3.10

Pore size distribution figures are attached in Appendix A of this document. Figure 4.34-Figure 4.45 show the adsorption and desorption pore size distributions of all supports and their corresponding catalysts. Upon addition of cobalt, all pore size distributions show a decrease in pore volume, while most of the overall pore size distribution trends remain the same. This is to be expected because cobalt is filling some of the volume, which used to be available for nitrogen adsorption. These results are in line with the data provided in Table 4.4. Figure 4.36 (3.0%La<sub>2</sub>O<sub>3</sub>-Al<sub>2</sub>O<sub>3</sub>) and Figure 4.37 (15%Co/3.0%La<sub>2</sub>O<sub>3</sub>-Al<sub>2</sub>O<sub>3</sub>) pore size distribution trend shifts slightly to the left upon addition of the cobalt, resulting in a smaller pore radius as well. This is also consistent with the data presented in Table 4.4.

Figure 4.40 through Figure 4.45 all provide pore size distributions on the reference catalysts and their corresponding supports. These pore size distributions include duplicate trends, which show that the pore size distributions are relatively repeatable, with minimal error.

### 4.3 Temperature Programmed Reduction

Figure 4.17 shows the TPR profiles of all three catalysts, which have a similar profile of two distinct reduction peaks. The first peak is attributed to the reduction of Co<sub>3</sub>O<sub>4</sub> to CoO oxide. The second broad peak represents the reduction from CoO to Co metal. The reductions step are  $\text{Co}_3\text{O}_4 + \text{H}_2 \rightarrow 3\text{CoO} + \text{H}_2\text{O}$  and  $3\text{CoO} + 3\text{H}_2 \rightarrow 3\text{Co}$

+3H<sub>2</sub>O. The second peak is typically about three times that of the first peak is in line with this viewpoint. Jacobs et al.<sup>34</sup> demonstrated this with the use of TPR-EXAFS and TPR-XANES.

The Zr doped alumina shows a significant widening of the second peak, while the La doped alumina shows only a slight widening of the second peak in comparison to the titanium-doped supported catalyst. This widening is attributed to the interaction of cobalt oxide (CoO) surface species with the support. The Ti doped alumina appears to have both peaks shifted furthest to the left, which is due to the Ti weakening the interaction between cobalt and the alumina and thereby facilitating the reduction.

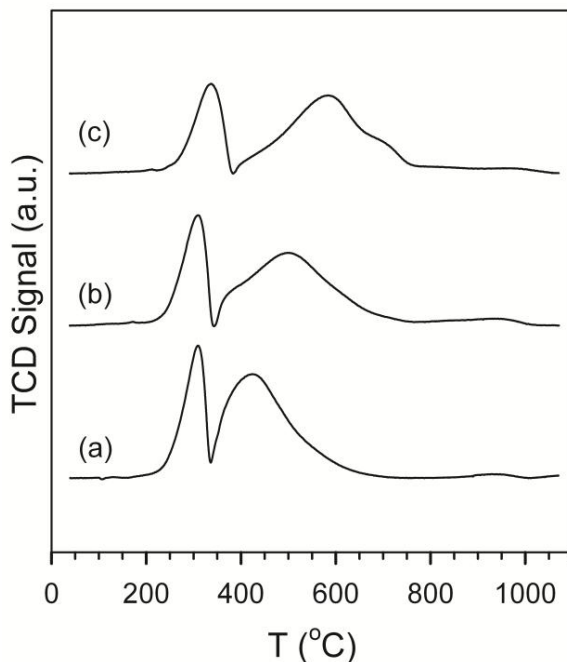


Figure 4.17: H-TPR profiles of, moving upward, (a) 15%Co/9.7%TiO<sub>2</sub>-Al<sub>2</sub>O<sub>3</sub>; (b) 15%Co/3.0%La<sub>2</sub>O<sub>3</sub>-Al<sub>2</sub>O<sub>3</sub>; and (c) 15%Co/3.1%ZrO<sub>2</sub>-Al<sub>2</sub>O<sub>3</sub>.

Figure 4.18 shows the TPR profile 15%Co/9.7%TiO<sub>2</sub>-Al<sub>2</sub>O<sub>3</sub> in comparison to two reference catalysts, 15%Co/Al<sub>2</sub>O<sub>3</sub> SBA 150 and 15%Co/Al<sub>2</sub>O<sub>3</sub> HF14/150. These references were chosen because the physisorption data suggests that they have comparable surface areas and pore sizes. As previously discussed, support surface area, pore volume, and pore radius can affect the performance of the catalysts, so Al<sub>2</sub>O<sub>3</sub> SBA 150 was chosen because it has a surface area lower (approximately 109m<sup>2</sup>/g), 9.7%TiO<sub>2</sub>-Al<sub>2</sub>O<sub>3</sub> has a surface area of approximately 137m<sup>2</sup>/g, and Al<sub>2</sub>O<sub>3</sub> HF14/150 has a surface area of approximately 152m<sup>2</sup>/g. This provides a high and a low point. In comparison to both reference catalysts, the catalyst with TiO<sub>2</sub> present has a distinct shift of the second reduction peak to lower temperatures.

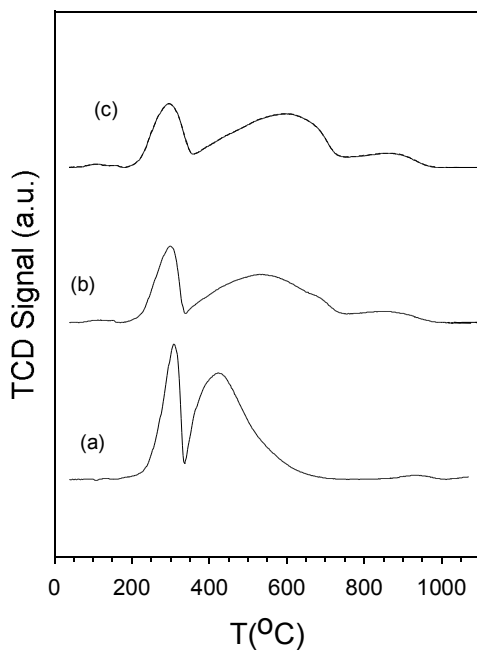


Figure 4.18: H-TPR profiles of, moving upward, (a) 15%Co/9.7%TiO<sub>2</sub>-Al<sub>2</sub>O<sub>3</sub>, (b) 15%Co/Al<sub>2</sub>O<sub>3</sub> SBA 150, and (c) 15%Co/Al<sub>2</sub>O<sub>3</sub> HF14/150

Figure 4.20 shows the TPR profile of 15%Co/3.1%ZrO<sub>2</sub>-Al<sub>2</sub>O<sub>3</sub> in comparison to two reference catalysts, 15%Co/Al<sub>2</sub>O<sub>3</sub> SBA 150 15%Co/Al<sub>2</sub>O<sub>3</sub> SBA 200. These reference catalysts were chosen for 15%Co/3.1%ZrO<sub>2</sub>-Al<sub>2</sub>O<sub>3</sub> because of the support surface area. According to this TPR profile, the presence of ZrO<sub>2</sub> in the support appears to cause a slight shift of the second reduction peak to lower temperatures.

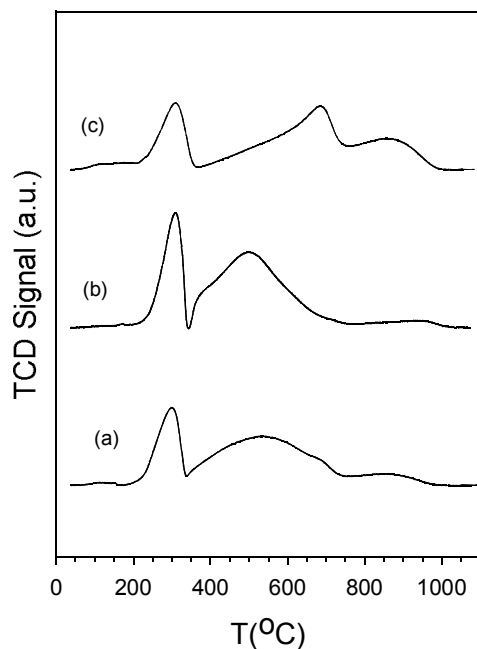


Figure 4.19: H-TPR profiles of, moving upward, (a) 15%Co/Al<sub>2</sub>O<sub>3</sub> SBA 150, (b) 15%Co/3.0%La<sub>2</sub>O<sub>3</sub>-Al<sub>2</sub>O<sub>3</sub>, and (c) 15%Co/Al<sub>2</sub>O<sub>3</sub> SBA 200

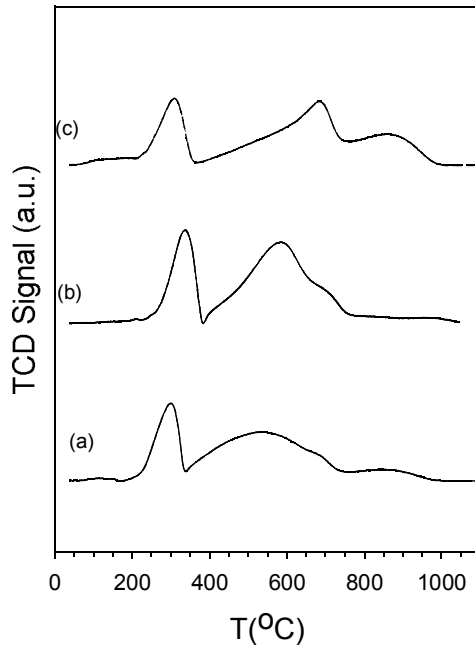


Figure 4.20: H-TPR profiles of, moving upward, (a) 15%Co/Al<sub>2</sub>O<sub>3</sub> SBA 150; (b) 15%Co/3.1%ZrO<sub>2</sub>-Al<sub>2</sub>O<sub>3</sub> and (c) 15%Co/Al<sub>2</sub>O<sub>3</sub> SBA 200.

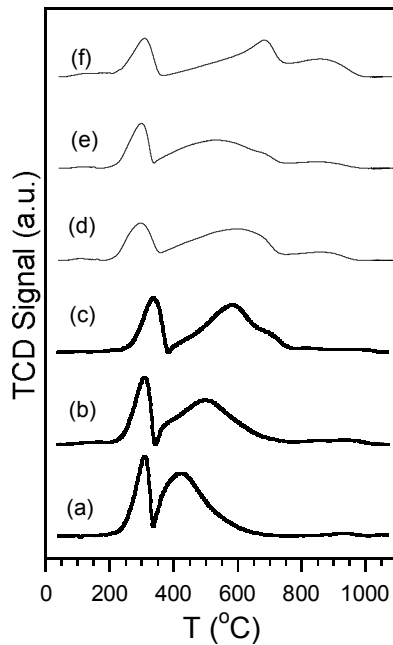


Figure 4.21: H-TPR profiles of, moving upward, (a) 15%Co/9.7%TiO<sub>2</sub>-Al<sub>2</sub>O<sub>3</sub>, (b) 15%Co/3.0%La<sub>2</sub>O<sub>3</sub>-Al<sub>2</sub>O<sub>3</sub>, (c) 15%Co/3.1%ZrO<sub>2</sub>-Al<sub>2</sub>O<sub>3</sub>, (d) 15%Co/Al<sub>2</sub>O<sub>3</sub> HP14/150, (e) 15%Co/Al<sub>2</sub>O<sub>3</sub> SBA150, and (f) 15%Co/Al<sub>2</sub>O<sub>3</sub> SBA200.

#### 4.4 Temperature Programmed Reduction After Reduction (TPR-AR)

The temperature programmed reduction after reduction profiles are shown as dashed lines along with the original TPR profiles in Figure 4.22. These profiles provide information on the amount of unreduced cobalt present on the surface, after the reduction step occurs. The titania promoted supported catalyst (a) profile corresponds to minimal unreduced cobalt, where lanthanum promoted (b) shows a small peak indicating a small fraction of cobalt remained unreduced. On the contrary, (c), zirconium promoted support, shows a significant amount of cobalt being reduced after reduction occurs.

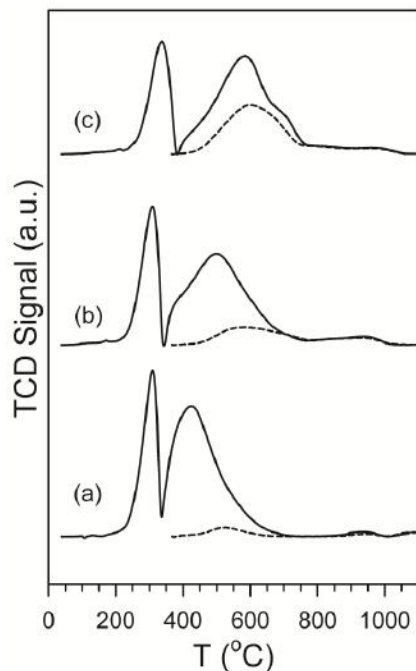


Figure 4.22: H-TPR (solid) and (dashed) H-TPR-AR profiles of, moving upward, (a) 15%Co/9.7%TiO<sub>2</sub>-Al<sub>2</sub>O<sub>3</sub>; (b) 15%Co/3.0%La<sub>2</sub>O<sub>3</sub>-Al<sub>2</sub>O<sub>3</sub>; and (c) 15%Co/3.1%ZrO<sub>2</sub>-Al<sub>2</sub>O<sub>3</sub>. Reduction was carried out in hydrogen for 10 hours at 350°C.

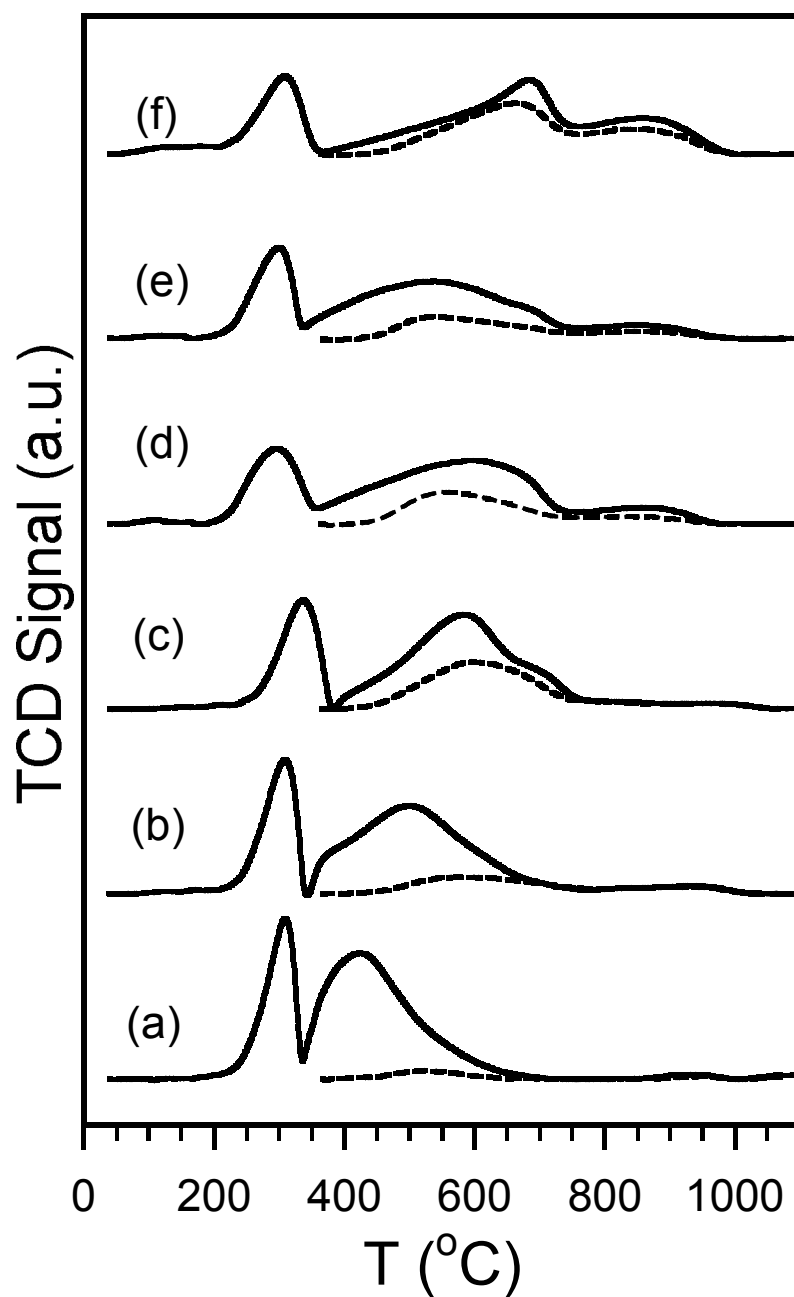


Figure 4.23: H-TPR (solid) and (dashed) H-TPR-AR profiles of, moving upward, (a) 15%Co/9.7%TiO<sub>2</sub>-Al<sub>2</sub>O<sub>3</sub>, (b) 15%Co/3.0%La<sub>2</sub>O<sub>3</sub>-Al<sub>2</sub>O<sub>3</sub>, (c) 15%Co/3.1%ZrO<sub>2</sub>-Al<sub>2</sub>O<sub>3</sub>, (d) 15%Co/Al<sub>2</sub>O<sub>3</sub> HP14/150, (e) 15%Co/Al<sub>2</sub>O<sub>3</sub> SBA150, and (f) 15%Co/Al<sub>2</sub>O<sub>3</sub> SBA200.

#### 4.5 Hydrogen Chemisorption

The hydrogen TPD results were used to calculate uncorrected dispersion. Uncorrected dispersion calculations are made under the assumption that all of the cobalt was reduced. In this calculation, it is assumed that one hydrogen atom attaches to one surface cobalt metal atom. The Altamira instrument provides hydrogen TPD results of  $\mu\text{mol } H_2$  desorbed. In order to determine the uncorrected dispersion the calculations are as follows.

$$\begin{aligned} \text{\# of } Co^0 \text{ moles on surface} &= 2 \times \mu\text{mol } H_2 \text{ desorbed} \times \frac{1 \text{ gmol}}{1E - 6 \mu\text{mol}} \\ \%D_{\text{uncor.}} &= \frac{\text{\# of } Co^0 \text{ moles on surface}}{\text{Total \# of moles of } Co \text{ in sample: i. e., bulk and surface}} \\ &= \frac{\text{\# of } Co^0 \text{ moles on surface}}{(\text{sample weight})(\text{wt\% of } Co^0 \text{ in sample})} \end{aligned}$$

TPD results provided data on the active site density of each catalyst. In assumption that we have one cobalt surface atom for every one hydrogen atom, we can use the amount of hydrogen desorbed to determine the active site density. The active site density is clearly presented in Figure 4.24, where the compared catalyst is in red and displayed on the x-axis and the reference catalysts are labeled in the graph legend. 15%Co/9.7%TiO<sub>2</sub>-Al<sub>2</sub>O<sub>3</sub> resulted in 66.3  $\mu\text{moles } H_2/\text{g}_{\text{cat}}$ , which also indicates 132.6  $\mu\text{moles surface cobalt}/\text{g}_{\text{cat}}$ . In reference to this catalyst's reference catalysts (15%Co/Al<sub>2</sub>O<sub>3</sub> HP14/150 and 15%Co/Al<sub>2</sub>O<sub>3</sub> SBA150), which resulted in

145.4 and 149.4  $\mu\text{moles surface cobalt/g}_{\text{cat}}$ . 15%Co/3.0%La<sub>2</sub>O<sub>3</sub>-Al<sub>2</sub>O<sub>3</sub> resulted in 142  $\mu\text{moles surface cobalt/g}_{\text{cat}}$ , in reference to this catalyst's reference catalysts (15%Co/Al<sub>2</sub>O<sub>3</sub> SBA150 and 15%Co/Al<sub>2</sub>O<sub>3</sub> SBA200), which resulted in 149.4 and 105.8  $\mu\text{moles surface cobalt/g}_{\text{cat}}$ . 15%Co/3.1%ZrO<sub>2</sub>-Al<sub>2</sub>O<sub>3</sub> resulted in 112.6  $\mu\text{moles surface cobalt/g}_{\text{cat}}$  in reference to this catalyst's reference catalysts (15%Co/Al<sub>2</sub>O<sub>3</sub> SBA150 and 15%Co/Al<sub>2</sub>O<sub>3</sub> SBA200), which resulted in 149.4 and 105.8  $\mu\text{moles surface cobalt/g}_{\text{cat}}$ . (15%Co/Al<sub>2</sub>O<sub>3</sub> SBA150 and 15%Co/Al<sub>2</sub>O<sub>3</sub> SBA200), which resulted in 149.4 and 105.8  $\mu\text{moles surface cobalt/g}_{\text{cat}}$ . At a first look, this appears to be a decrease in active site density as a result of increased cluster size on all three catalysts in question.

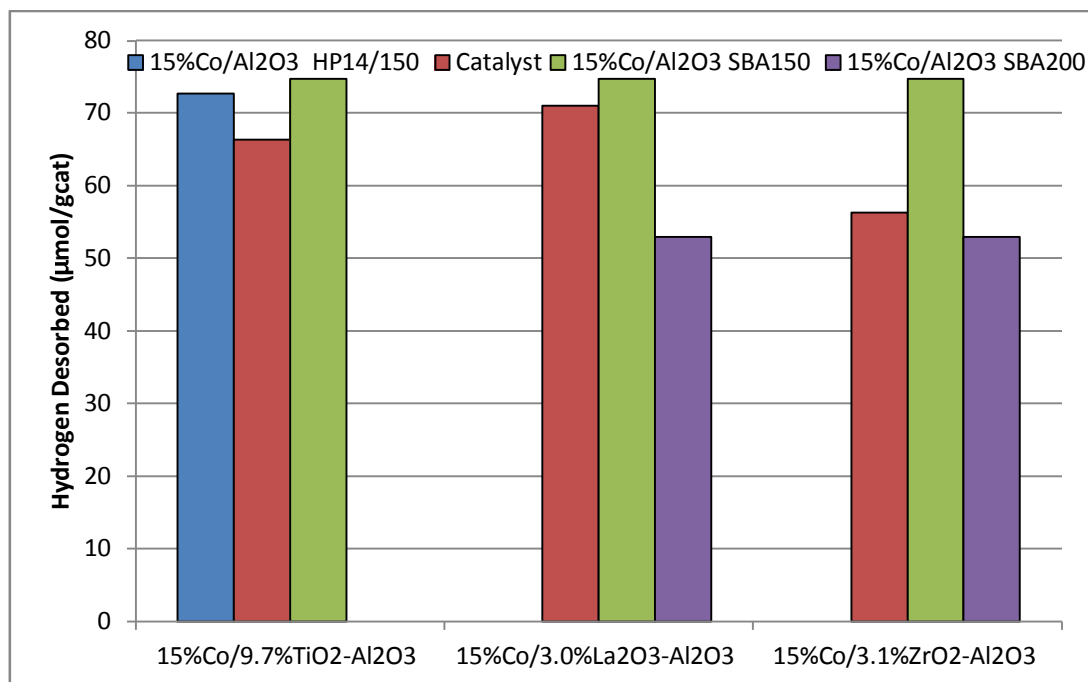


Figure 4.24: Temperature programmed desorption data for comparison of all catalysts with their corresponding reference catalysts.

The pulse reoxidation data is used to calculate the extent of reduction, which is then used to calculate the corrected dispersion, as follows. In this calculation, we assume that for every two oxygen molecules consumed, there are three moles of cobalt metal atom that were reduced.

$$\begin{aligned}
 & 3Co^0 + 2O_2 \rightarrow Co_3O_4 \\
 & \qquad \qquad \% \text{ Reduction} \\
 = & \frac{\# \text{ of } O_2 \text{ moles consumed during pulse reoxidation}}{\text{total \# of moles of Co in sample}} \left( \frac{3 \text{ moles } Co^0}{2 \text{ moles } O_2} \right) \\
 \%D_{cor.} = & \frac{\# \text{ of } Co^0 \text{ moles on surface}}{(\text{sample weight})(\text{wt\% of Co in sample})(\% \text{ Reduction})}
 \end{aligned}$$

Chemisorption results indicate that there was a wide range of reduction degree of the three doped alumina supported catalysts. Chemisorption, extent of reduction, dispersion and cluster size are shown in Table 4.5. Figure 4.25 through Figure 4.27 show some of the baseline data comparisons. Figure 4.25 shows the extent of reduction of each catalyst (red) in comparison to the relevant reference catalysts. Figure 4.26 shows the corrected cluster size of each doped support in comparison to each of the catalyst's reference catalyst cluster sizes. Similarly, Figure 4.27 shows the corrected dispersion for each of the catalysts in comparison to each reference catalyst.

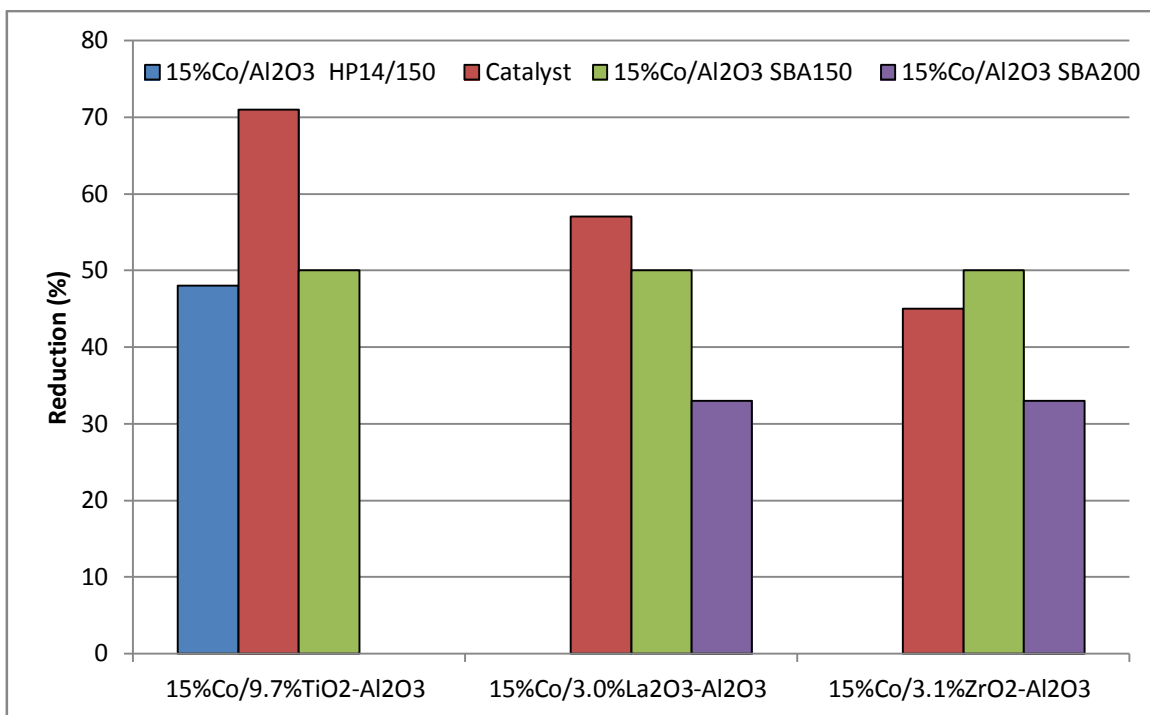


Figure 4.25: Extent of reduction results from pulse reoxidation testing for each catalyst in comparison to its corresponding reference catalyst.

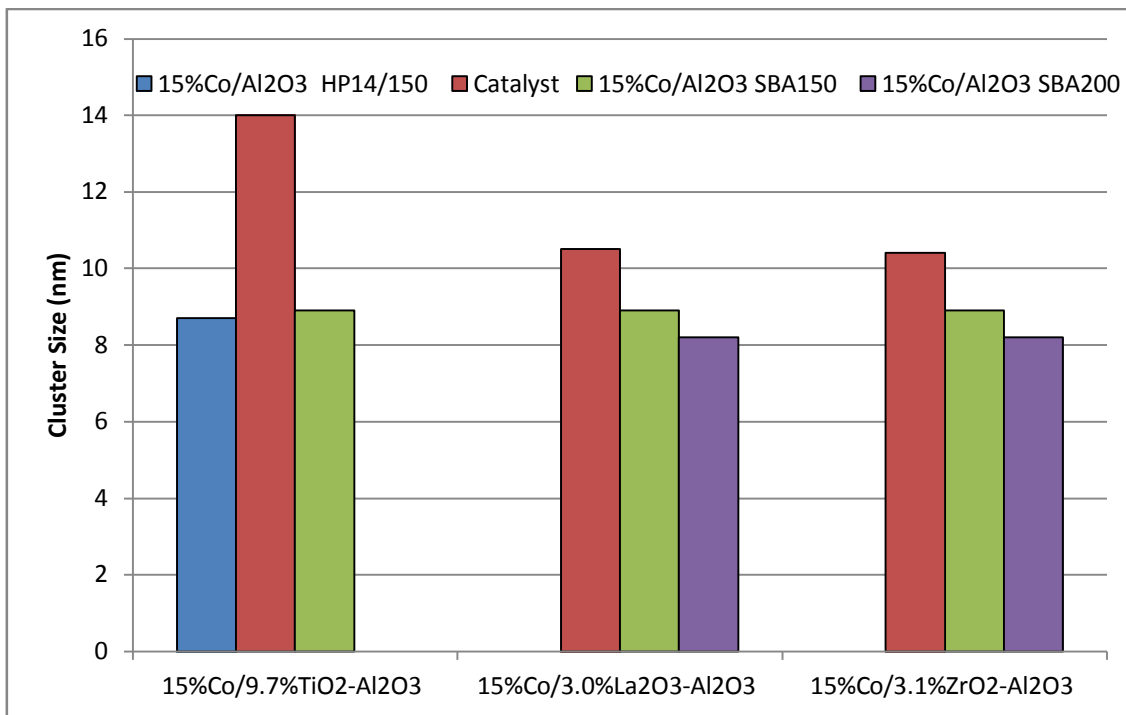


Figure 4.26: Pulse reoxidation cluster size data, which is corrected for extent of reduction for each catalyst in comparison to it's reference catalysts.

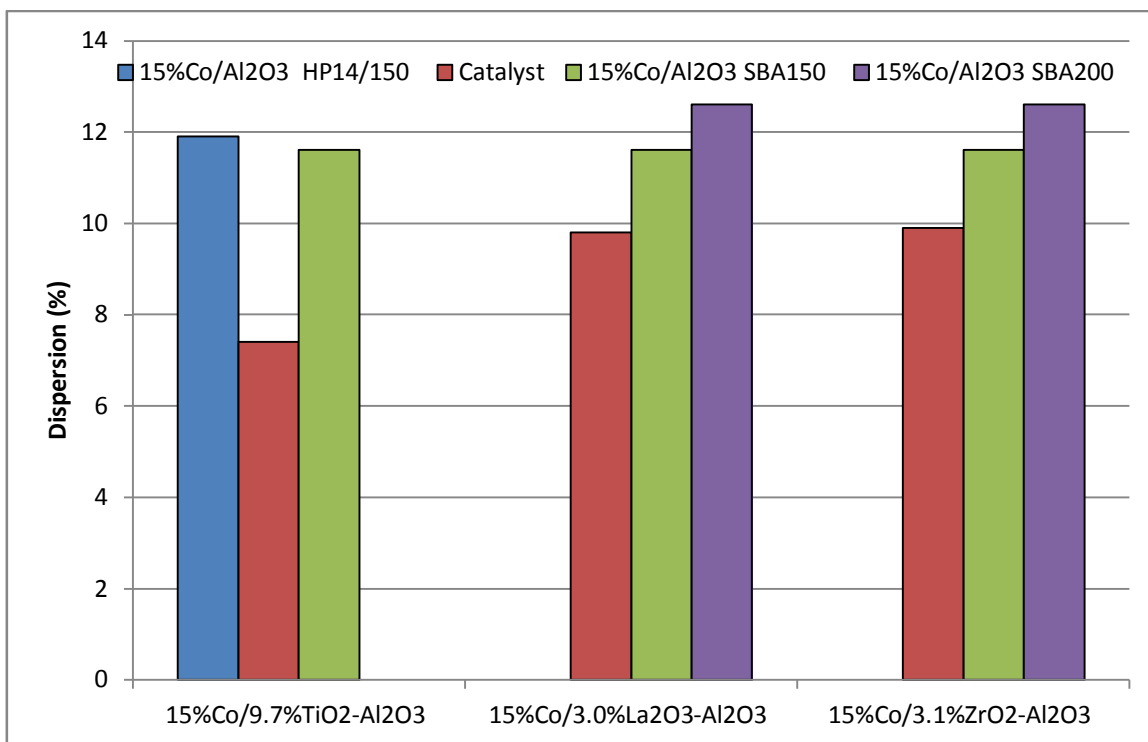


Figure 4.27: Corrected dispersion data for each catalyst in comparison to its reference catalysts

The TiO<sub>2</sub> doped alumina supported catalyst (15%Co/9.7%TiO<sub>2</sub>-Al<sub>2</sub>O<sub>3</sub>) had the largest cluster size (14 nm vs. 10.5/10.4nm) and the highest extent of reduction (71%). Since TiO<sub>2</sub> is known to have a weaker interaction with cobalt than pure alumina, this is consistent with what was expected. The larger average cluster size and increased extent of reduction on TiO<sub>2</sub> doped alumina are indicative of a weaker interaction with the support.

The cobalt cluster size and extent of reduction of 15%Co/3.0%La<sub>2</sub>O<sub>3</sub>-Al<sub>2</sub>O<sub>3</sub> and 15%Co/3.1%ZrO<sub>2</sub>-Al<sub>2</sub>O<sub>3</sub> were 10.5nm and 57% and 10.4nm and 45% respectively. Both the 15%Co/9.7%TiO<sub>2</sub>-Al<sub>2</sub>O<sub>3</sub> and 15%Co/3.0%La<sub>2</sub>O<sub>3</sub>-Al<sub>2</sub>O<sub>3</sub>

catalyst have a significantly higher extent of reduction than any of the reference catalysts and an increased cluster size. This which indicates that the cobalt-alumina interaction has been weakened.

Although 15%Co/3.1%ZrO<sub>2</sub>-Al<sub>2</sub>O<sub>3</sub> has a slightly lower extent of reduction (45%) than that of the two of the reference catalysts (15%Co/Al<sub>2</sub>O<sub>3</sub> SBA150, and 15%Co/Al<sub>2</sub>O<sub>3</sub> HP14/150) closely related to its properties (45% and 50%), it isn't clear if the zirconium has inhibited the reduction or not. These extent of reduction results are in line with the TPR-AR profiles.

Table 4.5: Hydrogen chemisorption / pulse reoxidation results following 10 hour hydrogen reduction at 350°C.

Catalyst Description	H <sub>2</sub> desorbed (μmoles/g <sub>cat</sub> )	D <sub>uncor</sub> (%)	d <sub>uncor</sub> (nm)	O <sub>2</sub> consumed (μmoles/g <sub>cat</sub> )	Red (%)	D <sub>cor</sub> (%)	d <sub>cor</sub> (nm)
15%Co/9.7% TiO <sub>2</sub> -Al <sub>2</sub> O <sub>3</sub>	66.3	5.2	19.8	1198	71	7.4	14.0
15%Co/3.0% La <sub>2</sub> O <sub>3</sub> -Al <sub>2</sub> O <sub>3</sub>	71.0	5.6	18.5	968	57	9.8	10.5
15%Co/3.1% ZrO <sub>2</sub> -Al <sub>2</sub> O <sub>3</sub>	56.3	4.4	23.3	757	45	9.9	10.4
15%Co/Al <sub>2</sub> O <sub>3</sub> HP14/150	72.7	18.1	5.71	816	48	11.9	8.7
15%Co/Al <sub>2</sub> O <sub>3</sub> SBA150	74.7	5.87	17.6	855	50	11.6	8.9
15%Co/Al <sub>2</sub> O <sub>3</sub> SBA200	52.9	4.15	24.8	558.5	33	12.6	8.2

#### 4.6 X-Ray Diffraction (XRD)

X-ray diffraction profiles are shown in Figure 4.28 through Figure 4.33. Each profile has labeled peaks for known components at the indicated angles. Simionato et al. have shown that the peak slightly below  $2\theta=20$  is corresponding to  $\text{Al}_2\text{O}_3$ <sup>35</sup>. The cobalt oxide peak located at  $2\theta=37^\circ$  was used to determine the crystallite size.

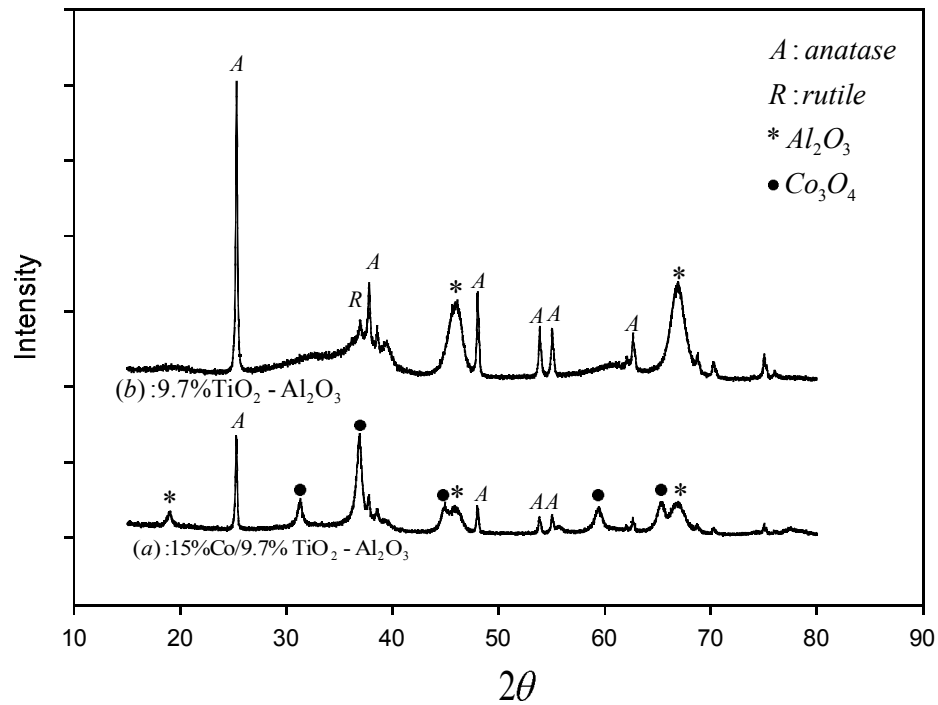


Figure 4.28: X-ray diffraction profile of 15%Co/9.7%TiO<sub>2</sub>-Al<sub>2</sub>O<sub>3</sub> (a) and 9.7%TiO<sub>2</sub>-Al<sub>2</sub>O<sub>3</sub> (b).

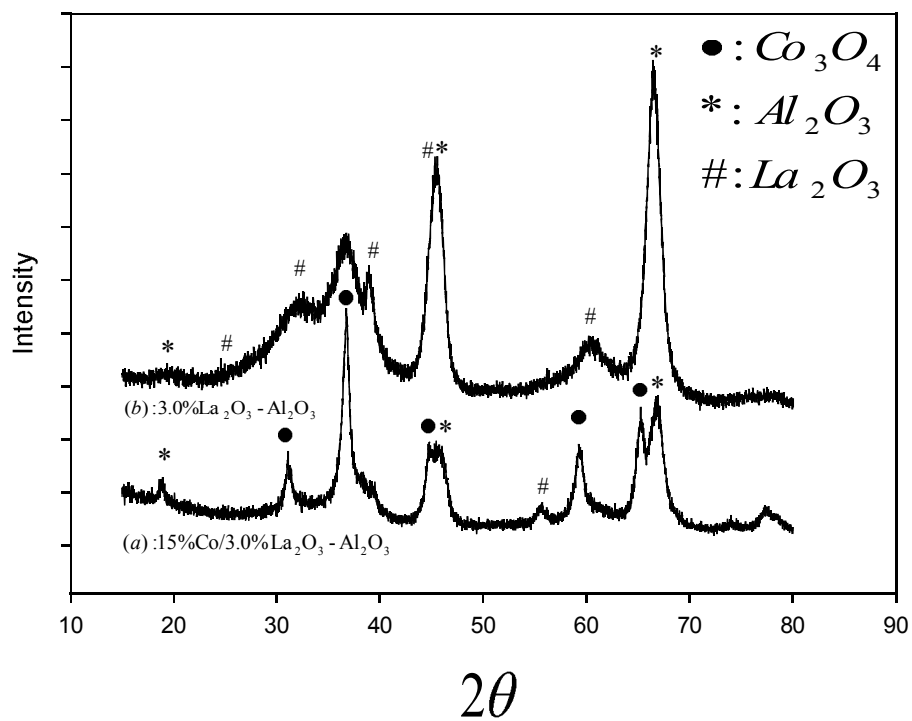


Figure 4.29: X-ray diffraction profiles of 15%Co/3.0%La<sub>2</sub>O<sub>3</sub>-Al<sub>2</sub>O<sub>3</sub> (a) and 3.0%La<sub>2</sub>O<sub>3</sub>-Al<sub>2</sub>O<sub>3</sub> (b).

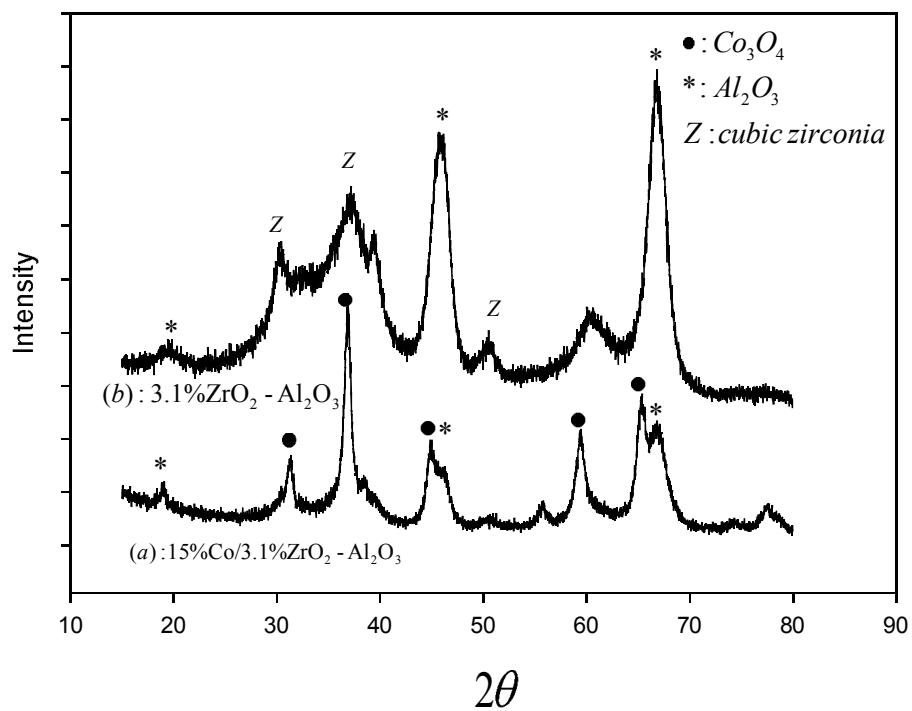


Figure 4.30: X-ray diffraction patterns of calcined samples 15%Co/3.1%ZrO<sub>2</sub>-Al<sub>2</sub>O<sub>3</sub> (a) and 3.1%ZrO<sub>2</sub>-Al<sub>2</sub>O<sub>3</sub> (b).

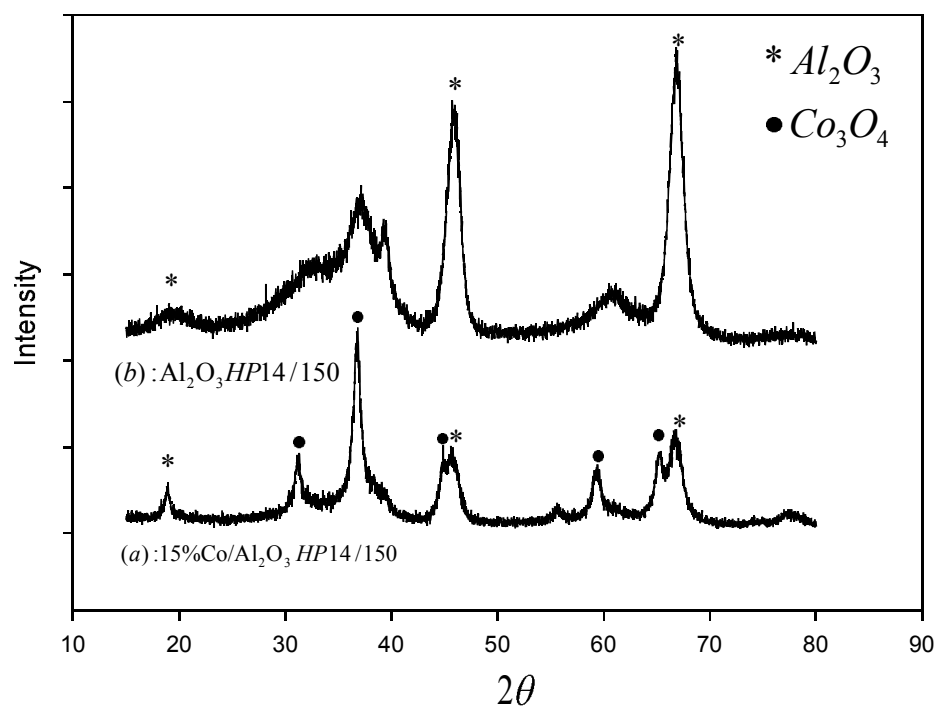


Figure 4.31: X-ray diffraction patterns of calcined samples 15%Co/ $\text{Al}_2\text{O}_3$  HP14/150 (a) and  $\text{Al}_2\text{O}_3$  HP14/150 (b).

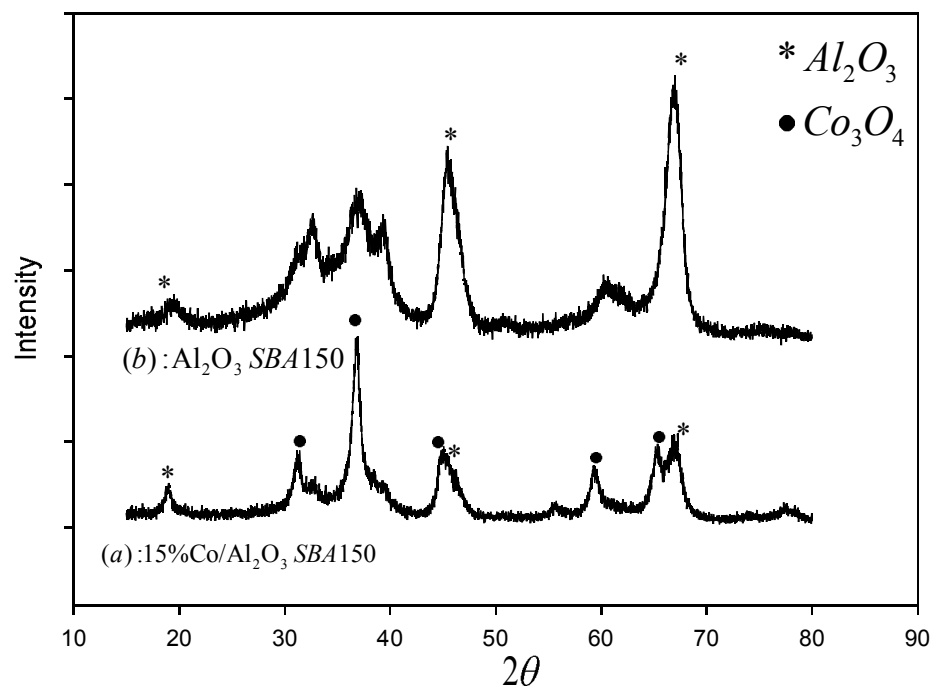


Figure 4.32: X-ray diffraction patterns of calcined samples 15%Co/ $\text{Al}_2\text{O}_3$  SBA150 (a) and  $\text{Al}_2\text{O}_3$  SBA150 (b).

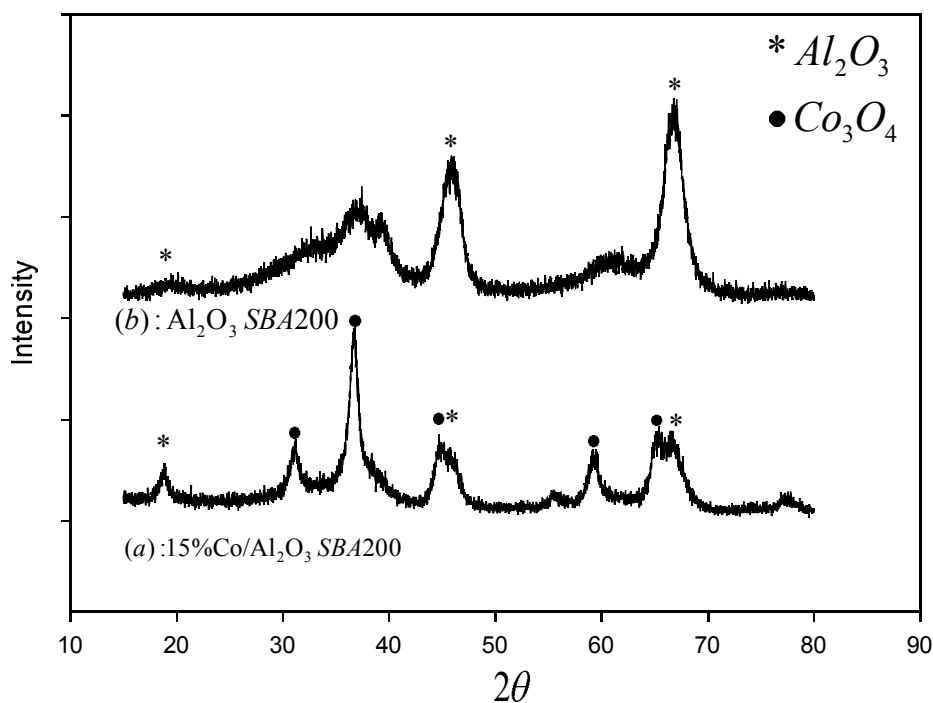


Figure 4.33: X-ray diffraction patterns of calcined samples 15%Co/ $Al_2O_3$  SBA200 (a) and  $Al_2O_3$  SBA200 (b).

Table 4.6 below shows the particle size estimate from XRD line broadening analysis at  $2\theta=37^\circ$  and using the Scherrer equation, as follows.

$$d = \frac{0.89\lambda}{B\cos\theta}$$

$d$ : average crystallite diameter

$\lambda$ : wavelength of the x – ray (1.54 Å)

$B$ : full width at half of the maximum intensity (in radians)

After reduction, it is expected that the cobalt cluster size should be around 75% of the original cobalt oxide cluster size, so a contraction factor of 0.75 was used

for converting  $\text{Co}_3\text{O}_4$  to  $\text{Co}^0$ . The results give expected cobalt metal cluster sizes for 15%Co/9.7% $\text{TiO}_2$ - $\text{Al}_2\text{O}_3$ , 15%Co/3.1% $\text{ZrO}_2$ - $\text{Al}_2\text{O}_3$ , and 15%Co/3.0% $\text{La}_2\text{O}_3$ - $\text{Al}_2\text{O}_3$  as 12.1 nm, 7.8 nm, and 8.5 nm, respectively. These results are in line with the chemisorption results previously discussed.

Table 4.6: X-ray Diffraction results from XRD plots and Scherrer Equation

Catalyst	Average diameter of $\text{Co}_3\text{O}_4$ domains (nm)	Expected average $\text{Co}^0$ domain diameter (nm) by applying 0.75 contraction factor
15%Co/9.7% $\text{TiO}_2$ - $\text{Al}_2\text{O}_3$	15.3	11.5
15%Co/3.0% $\text{La}_2\text{O}_3$ - $\text{Al}_2\text{O}_3$	11.7	8.8
15%Co/3.1% $\text{ZrO}_2$ - $\text{Al}_2\text{O}_3$	11.3	8.5
15%Co/ $\text{Al}_2\text{O}_3$ HP14/150	10.4	7.8
15%Co/ $\text{Al}_2\text{O}_3$ SBA150	9.9	7.4
15%Co/ $\text{Al}_2\text{O}_3$ SBA200	9.6	7.2

#### 4.7 Discussion

TPR profiles have indicated narrowing and a significant shift in the second reduction peaks to lower temperatures of both the  $\text{La}_2\text{O}_3$  and  $\text{TiO}_2$  doped supported catalysts. The TPR-AR profiles show that after reduction has occurred, these doped supports have significantly increased the active cobalt present on the surface of the support, in comparison to all three reference supported catalysts. Along with both TPR and TPR-AR results, the pulse reoxidation measurements of the hydrogen chemisorptions have confirmed these findings. The extent of reduction of the  $\text{La}_2\text{O}_3$  doped supported catalyst was 57% in comparison to referenced alumina supported

catalysts (48%, 50%, and 33%). The extent of reduction of the TiO<sub>2</sub> doped supported catalyst was 71%. In comparison to the referenced pure alumina supported catalysts, this is a significant increase in reducibility. All of these results indicate that both La<sub>2</sub>O<sub>3</sub> and TiO<sub>2</sub> doped supports have facilitated the reduction of cobalt oxide species in reference to pure alumina supported cobalt catalysts.

There was a slight shift in the second reduction peak of the ZrO<sub>2</sub> doped supported catalyst to a lower temperature, however TPR-AR results are not clear as to whether or not the reduction of ZrO<sub>2</sub> doped supported catalyst facilitated the reduction or not. In further investigation, the hydrogen chemisorption data resulted in an extent of reduction of 45% in comparison to pure alumina SBA150 and SBA200 (48% and 33% respectively). While it is not apparent that the doped ZrO<sub>2</sub> supported catalyst facilitated the reduction, it is also unclear whether or not it inhibited the reduction. Further investigation of the effect of ZrO<sub>2</sub> doping is necessary. A suggestion is that a better reference support is used in further research and that various doping levels of ZrO<sub>2</sub> on alumina are explored.

The hydrogen chemisorption and pulse reoxidation results have shown an increased corrected cluster size for all three doped supported catalysts. The pure alumina supported reference catalysts had corrected cluster size diameters of 8.2, 8.9, and 8.7 nanometers. The three doped supported catalysts: TiO<sub>2</sub>, La<sub>2</sub>O<sub>3</sub>, and ZrO<sub>2</sub> had corrected cluster size diameters of 14.0, 10.5, and 10.4 nanometers respectively. Although this may not be a significant increase in cluster size for all three doped supports, it has been shown that increasing the particle size to 10nm

may be beneficial from a stability standpoint<sup>36</sup>. It has also been shown that catalysts with smaller cluster size were found to have a permanent and more sensitive deactivation in the presence of water<sup>37</sup>. Never the less, the cluster size has been affected by the dopant being present on the support. Cobalt cluster size was also measured using XRD, which provided a cross reference for the pulse reoxidation data. The XRD data required the use of a contraction factor in order to compare the data, since XRD is completed on cobalt oxide and reduced cobalt metal. The results of XRD were in line with pulse reoxidation data.

Since the TiO<sub>2</sub> and La<sub>2</sub>O<sub>3</sub> doped supported catalysts have displayed an increase in reduction and an increase in the cluster size, it is likely that the support-metal interaction was weakened by the addition of TiO<sub>2</sub> and La<sub>2</sub>O<sub>3</sub>. ZrO<sub>2</sub> results in both reduction and cluster size data lead to the conclusion that the interaction was likely decreased upon presence of ZrO<sub>2</sub> on the alumina, but further investigation is recommended. Pore size distributions showed only a slight decrease in pore volume upon addition of cobalt to the supports in question. This likely means that the cobalt cluster size was dependent upon the surface interaction of cobalt oxide with the support, rather than the pore radius. On all three catalysts, TPD results provided a baseline for active site density. In comparison to their reference catalysts, all three catalyst showed a decrease in active site density, which was likely caused by the increased cobalt cluster size previously discussed.

The quality of data in this report appears to be high, multiple characterization techniques were compared and various techniques resulted in the

same conclusions. TPR results were in line with oxygen titration extent of reduction results, as well as XRD cluster size results agreeing with hydrogen chemisorptions and pulse reoxidation data. It is suggested that this research be continued in order to fully understand the impact these catalysts will have on Fischer-Tropsch synthesis. The catalyst characterization results indicate that the titanium oxide and lanthanum oxide doped alumina supported catalysts are of interest because of the weakened cobalt support interaction and potential decrease in catalyst cost. By increasing the extent of reduction, there is more metallic cobalt present on the support. However, whether or not there is more cobalt available to participate in the Fischer-Tropsch synthesis reaction (cobalt surface atoms) depends also on the cluster size in addition to the extent of reduction. On the one hand, while increasing cluster size alone tends to decrease the active site density, on the other hand, by increasing the size of the cobalt clusters, there is less likelihood of forming oxidized cobalt complexes, such as cobalt aluminate, during Fischer-Tropsch synthesis. Thus, from the standpoint of stability, improving the extent of reduction while increasing the particle size slightly may be beneficial for maintaining the sites, even if there is a slight decrease in overall initial site density. For catalysts with significant metal-support interactions, there is often a reduction promoter present in the form of a precious metal, like platinum. It is in the best interest of researchers to find ways to minimize the dependency on reduction promoters that are expensive metals, while at the same time increasing the performance of these cobalt catalysts<sup>3</sup>. These catalyst should be studied in a continuously stirred tank reactor to study their long term stability. The reaction kinetics will also provide data on activity and

selectivity, which will be useful in determining the overall catalytic improvements upon titanium and lanthanum oxide doping of alumina. As for zirconium oxide doped alumina supports, it is suggested that an in depth study be conducted, which has already begun. The goal of this study is to have a more representative reference support and that various amounts of zirconium oxide modifications be made to the alumina support. This study will provide information on the affect zirconium oxide has on the final cobalt catalyst and whether or not zirconium oxide inhibits reduction.

#### 4.8 Conclusions

TPR results indicated that both  $\text{La}_2\text{O}_3$  and  $\text{TiO}_2$  doped supports facilitated the reduction of cobalt oxide species in reference to pure alumina supported cobalt catalysts, however further investigation is needed to determine the effect of  $\text{ZrO}_2$  doping on the reduction profile. The hydrogen chemisorption/pulse reoxidation and XRD results have show an increased corrected cluster size for all three doped supported catalysts in comparison to their reference catalysts. Since the  $\text{TiO}_2$  and  $\text{La}_2\text{O}_3$  doped supported catalysts displayed an increase in reduction and an increase in the cluster size, it is likely that the support-metal interaction was weakened by the addition of  $\text{TiO}_2$  and  $\text{La}_2\text{O}_3$ . Results for  $\text{ZrO}_2$  were unclear whether zirconium oxide facilitated the reduction or inhibited it, but cluster size was slightly increased when zirconium oxide was present on the support. This leads to the conclusion that the interaction was likely decreased with the presence of  $\text{ZrO}_2$  on the alumina, but further investigation is recommended on a better representative support to determine how zirconium oxide affects the reduction of the cobalt catalysts.

Furthermore, pore size distributions showed only a slight decrease in pore volume upon addition of cobalt to the supports in question. This likely means that the cobalt cluster size was dependent upon the surface interaction of cobalt oxide with the support, rather than the pore radius, thus leading to a conclusion of weakened interaction between the doped supports and cobalt.

By increasing the extent of reduction, there is more metallic cobalt present on the support. However, whether or not there is more cobalt available to participate in the Fischer-Tropsch synthesis reaction (cobalt surface atoms) depends also on the cluster size in addition to the extent of reduction. On the one hand, while increasing cluster size alone tends to decrease the active site density, on the other hand, by increasing the size of the cobalt clusters, there is less likelihood of forming oxidized cobalt complexes, such as cobalt aluminate, during Fischer-Tropsch synthesis. Thus, from the standpoint of stability, improving the extent of reduction while increasing the particle size slightly may be beneficial for maintaining the sites, even if there is a slight decrease in overall initial site density. For catalysts with significant metal-support interactions, there is often a reduction promoter present in the form of a precious metal, like platinum. It is in the best interest of researchers to find ways to minimize the dependency on reduction promoters that are expensive metals, while at the same time increasing the performance of these cobalt catalysts<sup>3</sup>. The hypothesis was that the presence of lanthanum oxide, titanium oxide, and zirconium oxide on alumina oxide would reduce the interaction between cobalt and the alumina oxide support in Fischer-Tropsch catalysis. This hypothesis has been verified for both lanthanum oxide and

titanium oxide, but further studies are needed to verify the interaction affect of zirconium oxide. A follow-up study should be conducted using a reference alumina support and doping various amounts of zirconium oxide on the support and the reduction should be examined to see if there is variation in the reduction profile in correlation to the amount of zirconium oxide present.

## BIBLIOGRAPHY

- (1) Edwards, T.; Minus, D.; Harrison, W.; Corporan, E. In 40th AIAA/ASME/SAE/ASEE Joint Propulsion Conference and Exhibit 2004; Vol. 2004.
- (2) Bulzan, D., Anderson, Bruce In Proceedings of ASME Turbine Expo 2010: Power for Land, Sea and Air, GT2010 Glasgow, Scotland, 2010.
- (3) Atashi, H.; Siami, F.; Mirzaei, A. A.; Sarkari, M. Journal of Industrial and Engineering Chemistry **2010**, 16, 952.
- (4) Brunauer, S.; Emmett, P. H.; Teller, E. Journal of the American Chemical Society **1938**, 60, 309.
- (5) Lu, X.; Hildebrandt, D.; Liu, X.; Glasser, D. Industrial & Engineering Chemistry Research **2010**, 49, 9753.
- (6) Yao, Y.; Hildebrandt, D.; Glasser, D.; Liu, X. Industrial & Engineering Chemistry Research **2010**, 49, 11061.
- (7) Jacobs, G.; Das, T. K.; Zhang, Y.; Li, J.; Racoillet, G.; Davis, B. H. Applied Catalysis A: General **2002**, 233, 263.
- (8) Ma, W.; Jacobs, G.; Sparks, D. E.; Gnanamani, M. K.; Pendyala, V. R. R.; Yen, C. H.; Klettlinger, J. L. S.; Tomsik, T. M.; Davis, B. H. Fuel **2011**, 90, 756.
- (9) Khodakov, A. Y.; Lynch, J.; Bazin, D.; Rebours, B.; Zanier, N.; Moisson, B.; Chaumette, P. Journal of Catalysis **1997**, 168, 16.
- (10) Iglesia, E.; Soled, S. L.; Fiato, R. A.; Via, G. H. Journal of Catalysis **1993**, 143, 345.
- (11) Espinoza RL, V. J., van Berge PJ, Bolder FH; Sastech (Proprietary) Limited: Johannesburg, South Africa, 1998.
- (12) Wang, W. J.; Chen, Y. W. Applied Catalysis **1991**, 77, 223.
- (13) Murzin, D. Y. Chemical Engineering Science **2009**, 64, 1046.
- (14) Jacobs, G.; Ribeiro, M. C.; Ma, W.; Ji, Y.; Khalid, S.; Sumodjo, P. T. A.; Davis, B. H. Applied Catalysis A: General **2009**, 361, 137.
- (15) Khodakov, A. Y.; Chu, W.; Fongarland, P. Chemical Reviews **2007**, 107, 1692.
- (16) Mu, S.; Li, D.; Hou, B.; Chen, J.; Sun, Y. Catalysis Letters **2009**, 133, 341.

- (17) Liu, Y.; Hanaoka, T.; Miyazawa, T.; Murata, K.; Okabe, K.; Sakanishi, K. *Fuel Processing Technology*, **90**, 901.
- (18) Wan, G.; Duan, A.; Zhao, Z.; Jiang, G.; Zhang, D.; Li, R.; Dou, T.; Chung, K. H. *Energy & Fuels* **2008**, *23*, 81.
- (19) Vada, S.; Chen, B.; Goodwin, J. G. *Journal of Catalysis* **1995**, *153*, 224.
- (20) Ledford, J. S.; Houalla, M.; Proctor, A.; Hercules, D. M.; Petrakis, L. *The Journal of Physical Chemistry* **1989**, *93*, 6770.
- (21) Cai, Z.; Li, J.; Liew, K.; Hu, J. *Journal of Molecular Catalysis A: Chemical* **2010**, *330*, 10.
- (22) Zhang, Y.; Liew, K.; Li, J.; Zhan, X. *Catalysis Letters* **2010**, *139*, 1.
- (23) Moradi, G. R.; Basir, M. M.; Taeb, A.; Kiennemann, A. *Catalysis Communications* **2003**, *4*, 27.
- (24) ALI; #160; S.; CHEN; B.; GOODWIN; G., J. Zr promotion of Co/SiO<sub>2</sub> for Fischer-Tropsch synthesis; Elsevier: Amsterdam, PAYS-BAS, 1995; Vol. 157.
- (25) Rohr, F.; Lindvåg, O. A.; Holmen, A.; Blekkan, E. A. *Catalysis Today* **2000**, *58*, 247.
- (26) Feller, A.; Claeys, M.; Steen, E. v. *Journal of Catalysis* **1999**, *185*, 120.
- (27) Michalak, A.; Nowosielska, M.; Józwiak, W. *Topics in Catalysis* **2009**, *52*, 1044.
- (28) Ulín, C. A.; De Los Reyes, J. A.; Escobar, J.; Barrera, M. C.; Cortés-Jacome, M. A. *Journal of Physics and Chemistry of Solids* **2010**, *71*, 1004.
- (29) Xiong, H.; Zhang, Y.; Liew, K.; Li, J. *Journal of Molecular Catalysis A: Chemical* **2005**, *231*, 145.
- (30) Niemantsverdriet, J. W. *Spectroscopy in Catalysis*; Third ed.; WILEY-VCH, 2007.
- (31) Feltes, T. E.; Espinosa-Alonso, L.; Smit, E. d.; D'Souza, L.; Meyer, R. J.; Weckhuysen, B. M.; Regalbuto, J. R. *Journal of Catalysis* **2010**, *270*, 95.
- (32) Tao, C.; Li, J.; Zhang, Y.; Liew, K. Y. *Journal of Molecular Catalysis A: Chemical* **2010**, *331*, 50.

- (33) Barrett, E. P.; Joyner, L. G.; Halenda, P. P. *Journal of the American Chemical Society* **1951**, 73, 373.
- (34) Jacobs, G.; Ji, Y.; Davis, B. H.; Cronauer, D.; Kropf, A. J.; Marshall, C. L. *Applied Catalysis A: General* **2007**, 333, 177.
- (35) Simionato, M.; Assaf, E. M. *Materials Research* **2003**, 6, 535.
- (36) van Steen, E.; Claeys, M.; Dry, M. E.; van de Loosdrecht, J.; Viljoen, E. L.; Visagie, J. L. *The Journal of Physical Chemistry B* **2005**, 109, 3575.
- (37) Jacobs, G.; Patterson, P. M.; Das, T. K.; Luo, M.; Davis, B. H. *Applied Catalysis A: General* **2004**, 270, 65.

## APPENDIX A. Pore Size Distribution Profiles

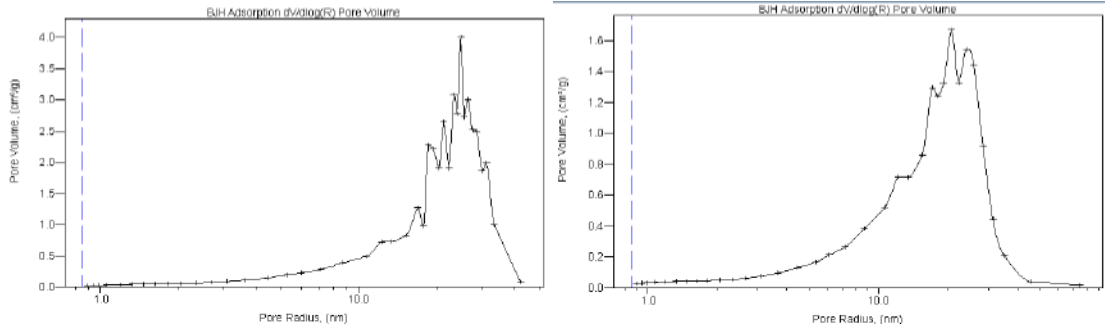


Figure 4.34: Adsorption pore size distribution of (left) 9.7%TiO<sub>2</sub>-Al<sub>2</sub>O<sub>3</sub> and (right) 15%Co/9.7%TiO<sub>2</sub>-Al<sub>2</sub>O<sub>3</sub>.

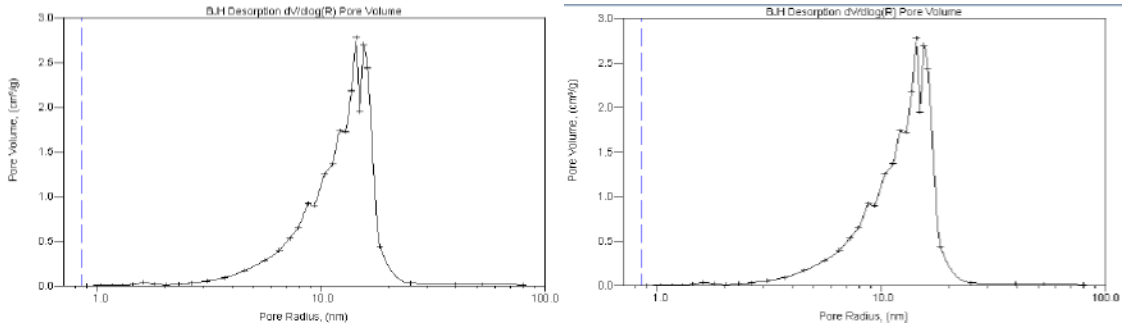


Figure 4.35: Desorption pore size distributions of 9.7%TiO<sub>2</sub>-Al<sub>2</sub>O<sub>3</sub>(left) and 15%Co/9.7%TiO<sub>2</sub>-Al<sub>2</sub>O<sub>3</sub>(right)

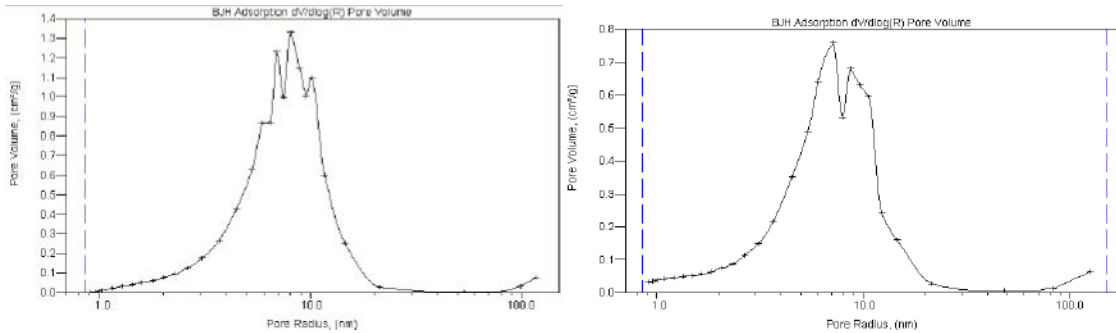


Figure 4.36: Adsorption pore size distribution of 3.0%La<sub>2</sub>O<sub>3</sub>-Al<sub>2</sub>O<sub>3</sub> (left) and 15%Co/3.0%La<sub>2</sub>O<sub>3</sub>-Al<sub>2</sub>O<sub>3</sub> (right)

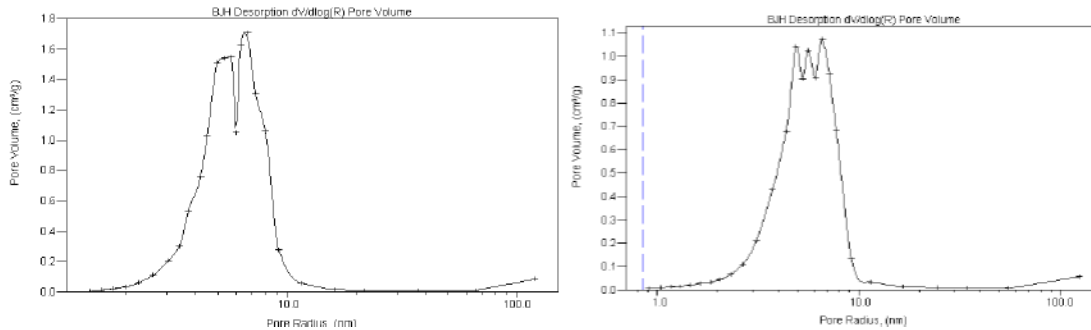


Figure 4.37: Desorption pore size distribution of 3.0%La<sub>2</sub>O<sub>3</sub>-Al<sub>2</sub>O<sub>3</sub> (left) and 15%Co/3.0%La<sub>2</sub>O<sub>3</sub>-Al<sub>2</sub>O<sub>3</sub> (right)

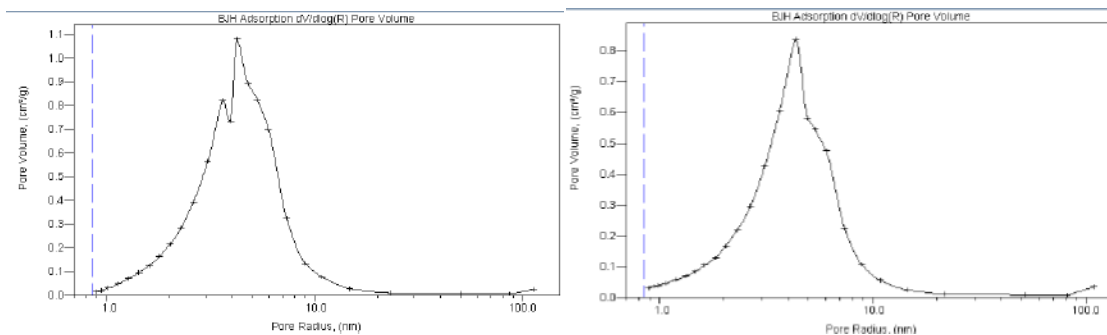


Figure 4.38: Adsorption pore size distribution of 3.1%ZrO<sub>2</sub>-Al<sub>2</sub>O<sub>3</sub> (left) and 15%Co/3.1%ZrO<sub>2</sub>-Al<sub>2</sub>O<sub>3</sub> (right)

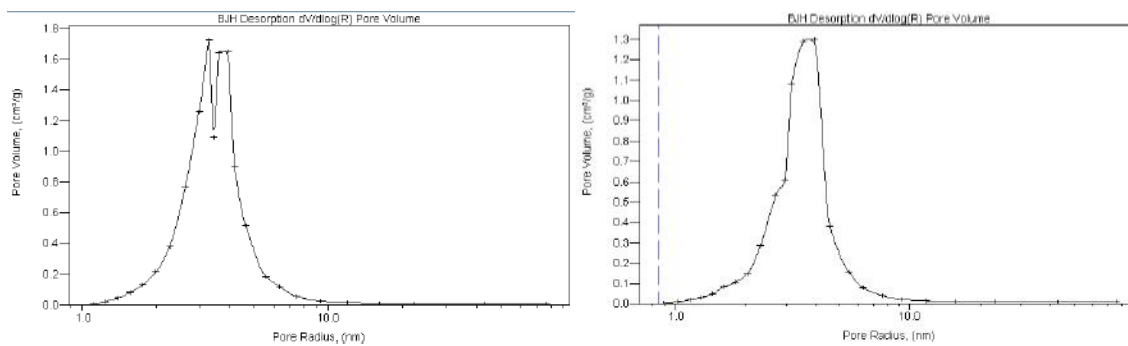


Figure 4.39: Desorption pore size distributions of 3.1%ZrO<sub>2</sub>-Al<sub>2</sub>O<sub>3</sub>(left) and 15%Co/3.1%ZrO<sub>2</sub>-Al<sub>2</sub>O<sub>3</sub> (right).

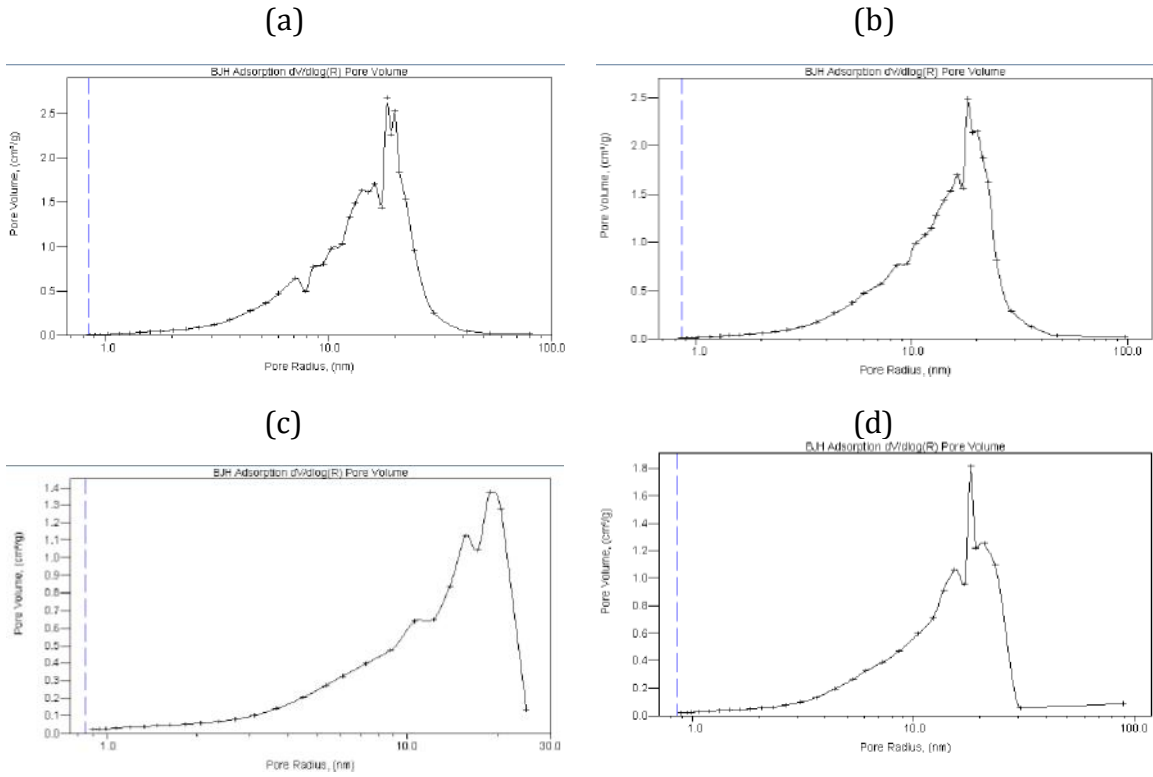


Figure 4.40: Adsorption pore size distribution of Al<sub>2</sub>O<sub>3</sub> HP14/150 (a) & (b) and 15%Co/Al<sub>2</sub>O<sub>3</sub> HP14/150 (c) & (d).

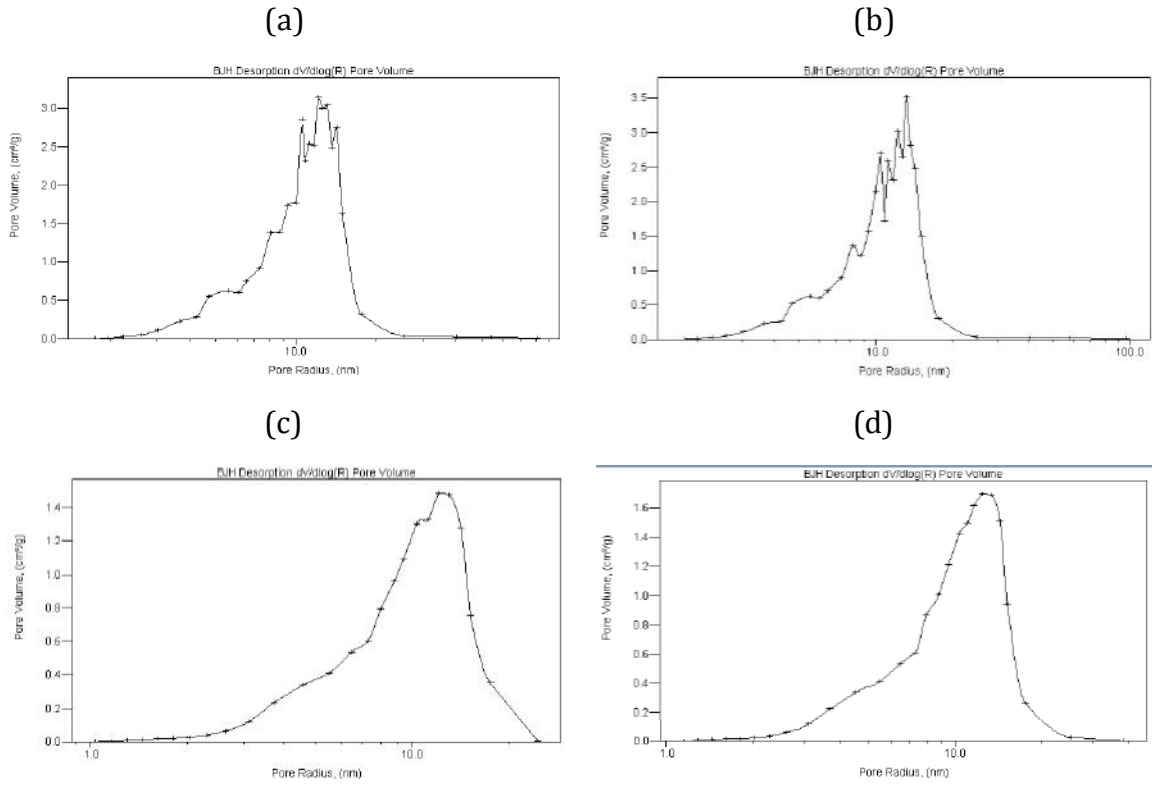


Figure 4.41: Desorption pore size distribution of  $\text{Al}_2\text{O}_3$  HP14/150 (a)& (b) and 15%Co/ $\text{Al}_2\text{O}_3$  HP14/150 (c) & (d).

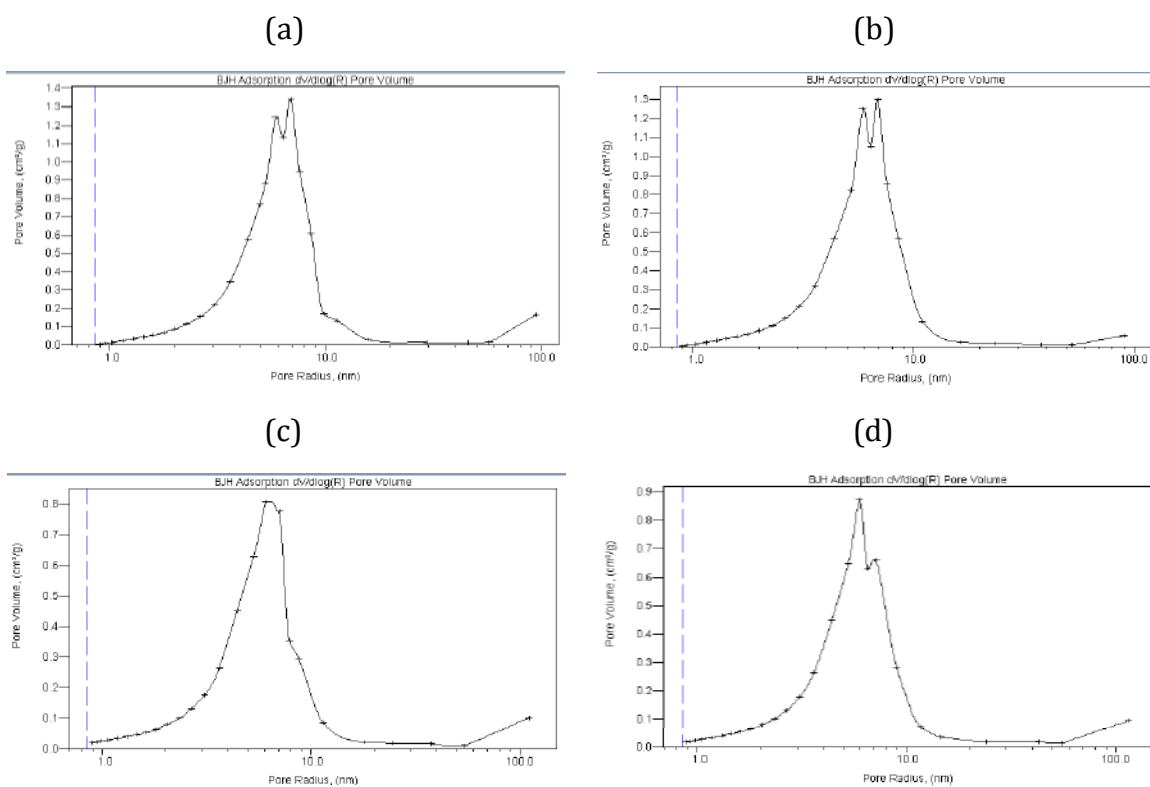


Figure 4.42: Adsorption pore size distributions of (a) & (b): SBA 150 Al<sub>2</sub>O<sub>3</sub> and (c) & (d): 15%Co/SBA 150 Al<sub>2</sub>O<sub>3</sub>.

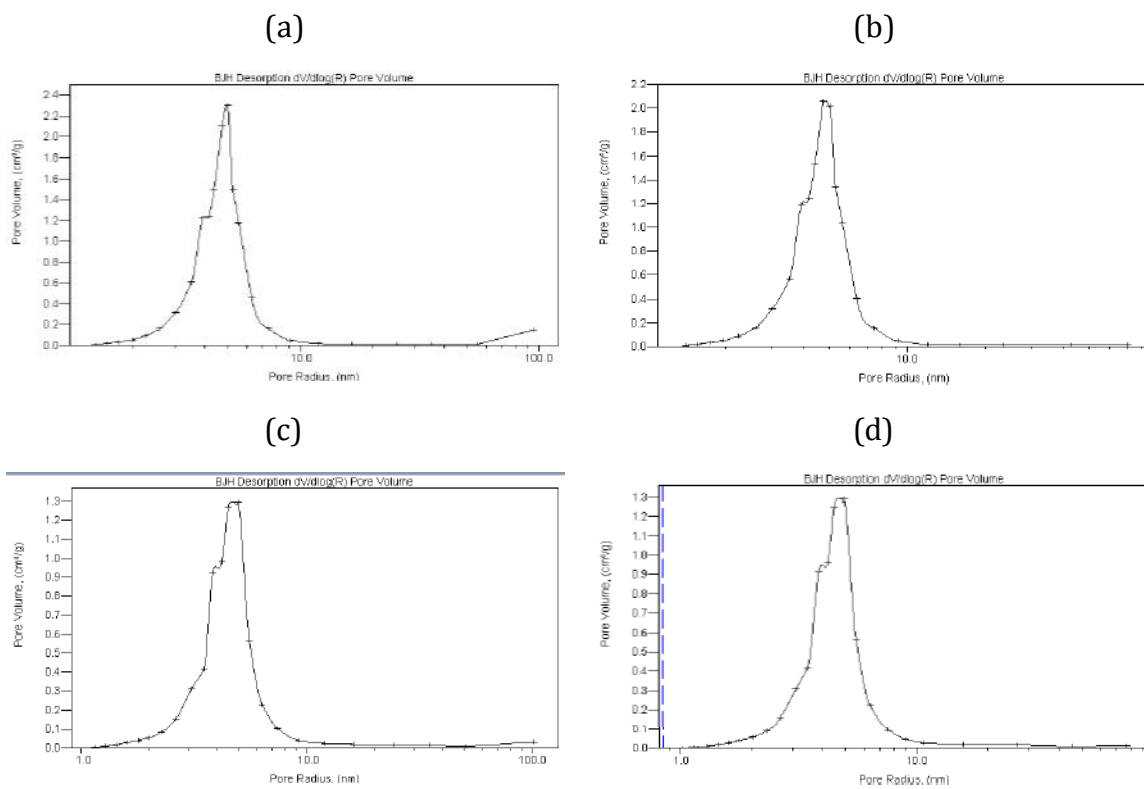


Figure 4.43: Desorption pore size distributions of (a) & (b): SBA 150 Al<sub>2</sub>O<sub>3</sub> and (c) & (d): 15%Co/SBA 150 Al<sub>2</sub>O<sub>3</sub>.

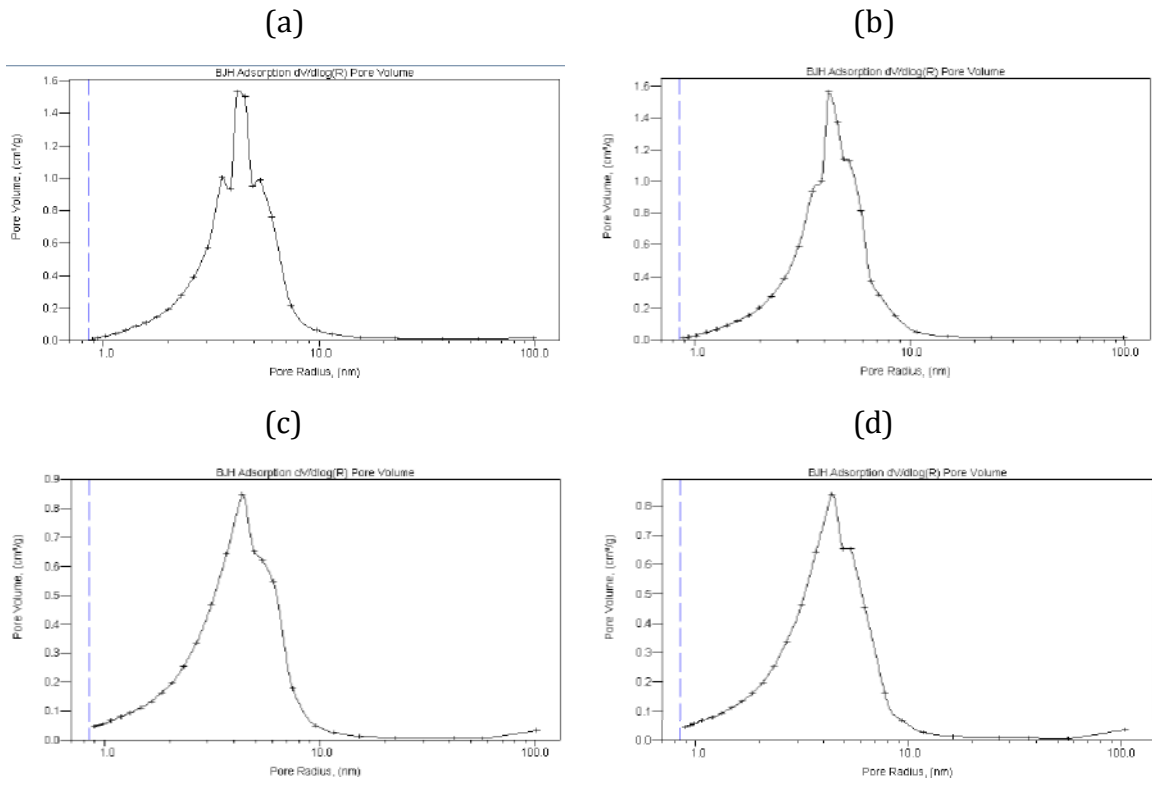


Figure 4.44: Adsorption pore size distributions of (a) & (b):  $\text{Al}_2\text{O}_3\cdot\text{SBA 200}$  and (c) & (d):  $15\%\text{Co}/\text{Al}_2\text{O}_3\cdot\text{SBA 200}$

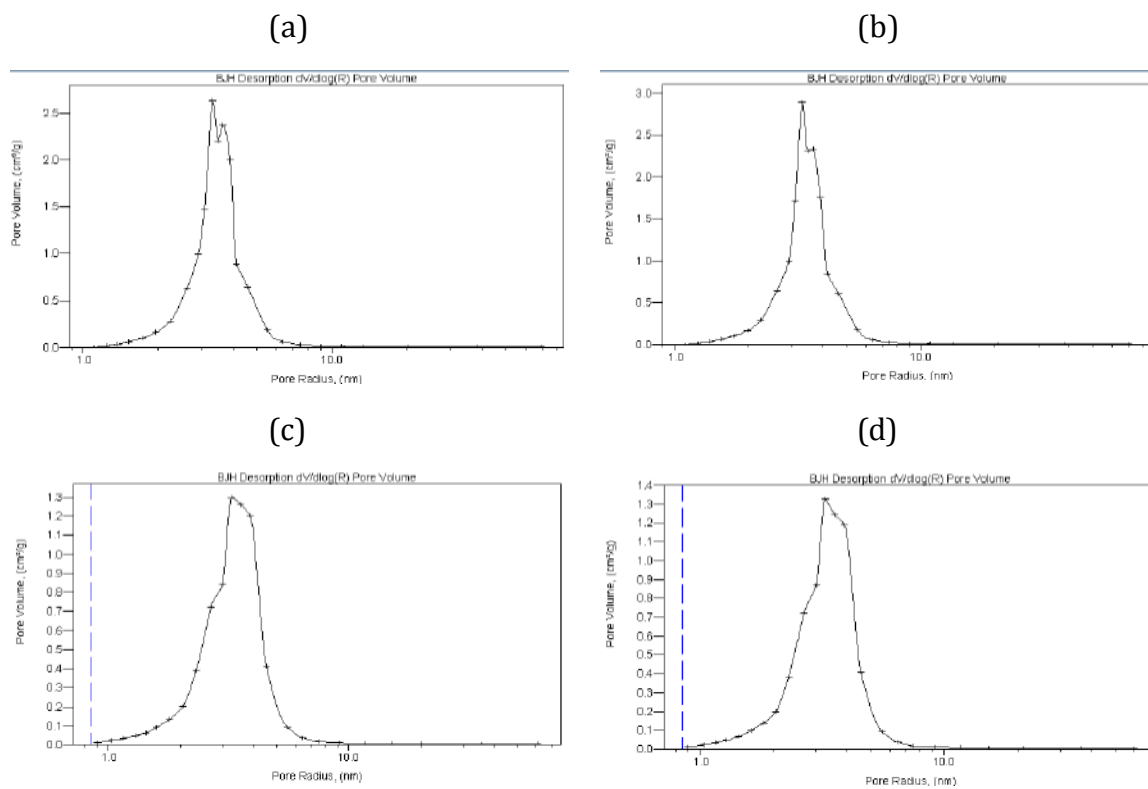


Figure 4.45: Desorption pore size distributions of (a) & (b):  $\text{Al}_2\text{O}_3\cdot\text{SBA 200}$  and (c) & (d): 15%Co/ $\text{Al}_2\text{O}_3\cdot\text{SBA 200}$

